

The structure of quark mass corrections in the $gg \rightarrow HH$ amplitude at high-energy

SEBASTIAN JASKIEWICZ^a, STEPHEN JONES^b, ROBERT SZAFRON^c, YANNICK
ULRICH^{a,d}

^a *Albert Einstein Center for Fundamental Physics, Institut für Theoretische Physik,
Universität Bern, Sidlerstrasse 5, CH-3012 Bern, Switzerland*

^b *Institute for Particle Physics Phenomenology, Durham University,
South Road, Durham, DH1 3LE, United Kingdom*

^c *Department of Physics, Brookhaven National Laboratory,
Upton, New York, 11973, U.S.A.*

^d *Department of Mathematical Sciences, University of Liverpool,
Liverpool, L69 3BX, United Kingdom*

Abstract

The leading and next-to-leading order QCD predictions for Higgs boson pair production at hadron colliders suffer from a significant mass renormalisation scheme uncertainty related to the choice of the top-quark mass. The functional dependence of the result on the value of the intermediate quark mass can be understood in the high-energy limit using the Method of Regions and the tools of Soft-Collinear Effective Theory. In this work, we study the origin of the sizeable logarithmic mass corrections in the $gg \rightarrow HH$ amplitudes at leading and next-to-leading power in the limit $s, |t|, |u| \gg m_t^2 \gg m_H^2$. We argue that the mass corrections follow a predictable factorised pattern that can be exploited to simplify their computation. We present results for the leading power leading logarithmic corrections, our analysis leads to a significant reduction in the theoretical uncertainty of the double Higgs production amplitudes at high-energy due to the top-quark mass scheme.

Contents

1	Introduction	1
2	Structure of the amplitudes at fixed order	3
2.1	Structure of the scalar integrals	5
2.1.1	One-loop	6
2.1.2	Two-loop	10
2.1.3	Three-loop and beyond	14
2.2	Structure of the one-loop amplitude	15
2.3	Structure of the two-loop amplitude	17
3	All-order factorisation in Effective Field Theory	18
3.1	Hard scale $\mu^2 \sim s$	20
3.1.1	Leading power matching	21
3.1.2	Next-to-leading power matching	22
3.2	Scale $\mu^2 \sim m_t^2$	27
3.2.1	Leading power amplitude	27
3.2.2	Next-to-leading power amplitude	29
3.3	Resummation	31
4	Controlling scheme uncertainties	33
5	Summary and outlook	40
A	Renormalisation and decoupling constants	42
B	Region expansion at two-loops	43
C	Amplitudes: Full vs Leading Power	45

1 Introduction

Computing multi-loop scattering amplitudes that retain the complete mass dependence for intermediate and initial/final state particles is exceptionally challenging. The current state-of-the-art for high multiplicity massive processes includes $2 \rightarrow 3$ results for $Wb\bar{b}$ [1–3], $Hb\bar{b}$ [4, 5], $Ht\bar{t}$ [6–8], Wjj [2], $W\gamma j$ [9], $Z\gamma\gamma$ [10], and $W\gamma\gamma$ [11] at two-loops. The relevant master integrals are known for five-point one mass [12, 13] and two-mass processes in the planar limit/leading-colour approximation [14, 15] (partly relying on generalised series solutions [16, 17]). In many cases, including Higgs boson pair production, fully analytic results have not been obtained for all Feynman integrals appearing beyond one-loop, and numerical [18, 19] or semi-numerical [16, 20, 21] methods are used either exclusively or to supplement partial analytic results.

For Higgs production processes in the limit of large intermediate quark mass ($m_q \rightarrow \infty$), a heavy top effective field theory has been constructed [22–24] in which massive quark loops are integrated out of the theory and effective couplings are introduced between the Higgs boson and gluons. The existence of such an effective theory means that higher-order corrections can be computed much more straightforwardly, with the quark mass dependence factorising from the loop integrals. This effective field theory approximation has been used extensively in Higgs physics and played an essential role in many high-order results in the literature, for example, the N³LO QCD corrections to Higgs boson production [25, 26]. Fixed-order QCD corrections for Higgs boson pair production are known at N³LO in the limit of large top-quark mass [27–29], which are not applicable for production of a Higgs pair with large total invariant mass.

Results for the partial and full electroweak corrections to Higgs pair production have also recently been obtained [30–33]. The corrections are also known in the limit of large top-quark mass [34] and the high-energy limit for the Yukawa corrections [35]. Retaining the complete top-quark mass dependence, the QCD corrections to Higgs boson pair production are known only at NLO [36–43]. The light-fermion n_f -contributions have been calculated at NNLO for forward scattering kinematics neglecting the Higgs boson mass [44]. Recently, the one-particle reducible contributions were also computed at NNLO [44, 45].

In Ref. [39], it was noted that the NLO result is sensitive to the precise value chosen for the intermediate top-quark mass and that the reduction in this dependence going from LO to NLO was mild. This behaviour means that small changes to the top-quark mass can enormously impact the NLO correction. Furthermore, the choice of the renormalisation scheme for the top-quark mass can have a sizable effect on the value obtained for the NLO result.

Taking the difference between results obtained using the on-shell (OS) and $\overline{\text{MS}}$ schemes for the top-quark mass as a genuine theoretical uncertainty leads to the introduction of a *mass scheme* uncertainty that is comparable in size to the usual renormalisation/factorisation scale uncertainties [41]. The renormalisation scale uncertainty can be significantly reduced using higher-order computations in the heavy top effective field theory described above; however, the mass scheme uncertainty can not be addressed in this limit, so it becomes the dominant theoretical uncertainty on Higgs pair production. The same fate is known to be suffered by several other amplitudes in the Higgs sector, including off-shell Higgs boson production [46, 47], Z -Higgs production [48, 49] and ZZ production via an intermediate Higgs boson.

Owing to the complexity of the NLO QCD corrections to Higgs pair production and the fact that they are known only numerically, significant effort has been invested to obtain results in various limits, namely,

1. High-energy limit¹: $s, |t|, |u| \gg m_t^2 \gg m_H^2$ [50–53],
2. Small Higgs boson mass limit: $s, |t|, |u| \gg m_H^2$ [54, 55],

¹Note that the term “high-energy limit” is often synonymous with the forward scattering – or Regge – limit where $-t/s \ll 1$, in this work we do not impose a hierarchy between the kinematic invariants.

3. Small- p_T and/or small- t [53, 56],
4. Near to the top-quark threshold: $s \sim 4m_t^2$ [57].

In this work, we focus on the first of these approximations and investigate to what extent the behaviour of the mass corrections in this limit can be understood using the Method of Regions (MoR) approach [58–61], Soft-Collinear Effective Field Theory (SCET) [62–66] and related tools [67–74]. Similar analyses have been carried out for the single Higgs boson production and decay amplitudes [75–87], Higgs boson plus jet [88] and power-enhanced QED corrections for $B_s \rightarrow \bar{\ell}\ell$ [89, 90].

In Section 2, we describe the general structure of the $gg \rightarrow HH$ amplitudes at fixed order, first by analysing the regions present in the scalar integrals and then discussing how the regions contribute at the amplitude level at one- and two- loop level. In Section 3, we introduce a SCET-based analysis of mass corrections to $gg \rightarrow HH$ and describe how the leading-power (LP) and next-to-leading power (NLP) mass effects can be resummed. In Section 4, we discuss to what extent the leading and sub-leading mass effects capture the mass dependence of the amplitude at high-energy and show how resumming the leading mass corrections reduces the mass scheme uncertainty. Finally, Section 5 presents our conclusions and outlook.

2 Structure of the amplitudes at fixed order

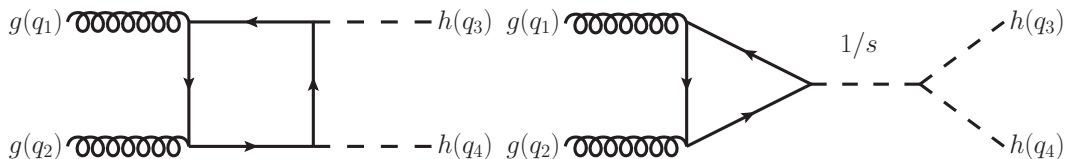


Figure 1: The leading order QCD diagrams contributing to $gg \rightarrow HH$. The left (box) diagram is proportional to y_t^2 , while the right (triangle) diagram is proportional to y_t .

We consider the process $g(q_1)g(q_2) \rightarrow H(-q_3)H(-q_4)$, with all momenta defined to be incoming. The amplitude can be parametrised in terms of the usual Mandelstam invariants,

$$s = (q_1 + q_2)^2, \quad t = (q_1 + q_3)^2, \quad u = (q_2 + q_3)^2. \quad (2.1)$$

The $gg \rightarrow HH$ amplitude can be decomposed in terms of two form factors, which can be chosen to be the helicity amplitudes, $A_1 = -\mathcal{M}^{++} = -\mathcal{M}^{--}$, and $A_2 = -\mathcal{M}^{+-} = -\mathcal{M}^{-+}$. Furthermore, the QCD corrections can be separated into *box* diagrams, A_{i,y_t^2} , in which both Higgs bosons couple to a massive quark line and *triangle* diagrams, $A_{i,y_t\lambda_3}$, in which a single off-shell Higgs boson couples to the massive quark line and splits into

two Higgs bosons via a trilinear self-coupling (here, for simplicity, we consider only the top quark to be massive). Explicitly,

$$A_1 = T_F \frac{G_F \alpha_s}{\sqrt{2} 2\pi} s \left[\frac{3m_H^2}{s - m_H^2} A_{1,y_t\lambda_3} + A_{1,y_t^2} \right], \quad A_2 = T_F \frac{G_F \alpha_s}{\sqrt{2} 2\pi} s [A_{2,y_t^2}]. \quad (2.2)$$

The form factors can then be further expanded in powers of the strong coupling as

$$A_{i,j} = \sum_{k=0} \left(\frac{\alpha_s}{2\pi} \right)^k A_{i,j}^{(k)}, \quad i = 1, 2, \quad j = y_t^2, y_t\lambda_3. \quad (2.3)$$

Representative leading-order diagrams are shown in Fig. 1.

We will focus on the behaviour of the amplitudes in the high-energy limit,

$$s, |t|, |u| \gg m_t^2 \gg m_H^2. \quad (2.4)$$

Since, from the perspective of QCD, the dependence on m_H^2 is only through the external kinematical invariants and the s -channel propagator in the triangle-type contribution, we will focus on the m_t mass dependence and take $m_t^2 \gg m_H^2$, i.e. we first set $m_H = 0$ and then perform expansion in the small top-mass, m_t . Restoring the kinematical dependence on m_H is straightforward after factorisation of the amplitude at the scale m_t . We define our power counting parameter as $\lambda = m_t/Q$, where Q is of the order of large invariants $s, |t|, |u|$.

We expand the amplitude around a small Higgs boson mass, $m_H \sim 0$. To leading power in the m_H expansion, this means that external momenta and Mandelstam invariants obey,

$$q_1^2 = q_2^2 = q_3^2 = q_4^2 = 0, \quad s + t + u = 0. \quad (2.5)$$

The contribution of the triangle-type ($y_t\lambda_3$) diagrams is power-suppressed by m_H^2/s relative to the box amplitude. For this case, the all-order structure of the mass-logarithms can be obtained from existing results for single Higgs production [78, 84–86, 91], and therefore we do not discuss it further.

The starting point of this work is the observation that the result for one- and two-loop box contributions to the $gg \rightarrow HH$ amplitude in the OS scheme can be written in the high-energy limit as [39, 40, 51],

$$A_{i,y_t^2}^{(0)} = y_t^2 f_i(s, t) + \mathcal{O}(y_t^2 m_t^2), \quad (2.6)$$

$$A_{i,y_t^2}^{(1)} = 3C_F A_i^{(0)} \log \left[\frac{m_t^2}{s} \right] + y_t^2 g_i(s, t) + \mathcal{O}(y_t^2 m_t^2), \quad (2.7)$$

where g_i does not depend on m_t . The functions f_i are the leading order leading power (in m_t) expressions for the form factors, explicitly they are given by [51],

$$f_1 = \frac{8}{s}, \quad f_2 = \frac{2}{st(s+t)} \left[-l_{1ts}^2 (s+t)^2 - l_{ts}^2 t^2 - \pi^2 (s^2 + 2st + 2t^2) \right], \quad (2.8)$$

and

$$l_{ts} = \log\left(-\frac{t}{s}\right) + i\pi, \quad l_{1ts} = \log\left(1 + \frac{t}{s}\right) + i\pi. \quad (2.9)$$

The appearance of a leading C_F term at two-loops can be understood as originating from the mass renormalisation counter-term as can be seen by converting the top-quark mass to the $\overline{\text{MS}}$ scheme [40]. Since the leading mass-dependent logarithm comes only from the mass counter-term, we can predict the leading behaviour of $A_{i,y_t}^{(1)}$ in the small mass limit just from the leading order $A_{i,y_t}^{(0)}$ result and the mass renormalisation counter-term.

Having noted the above, the immediate questions are,

1. Why does the box amplitude have such a simple structure?
2. Can super-leading/power-enhanced m_t terms appear in the integrals at higher loops, and can they spoil this picture?

In other words, we wish to establish whether or not the simple structure observed at one- and two-loop order persist to all orders in the QCD coupling.

To answer the above questions, we begin by analysing the process using the MoR and write down the modes and regions that contribute at each order in the power expansion in the quark mass. In the first step, we study individual scalar integrals, then we analyse complete amplitudes. In Section 3, using the understanding gained from the MoR analysis, we use the tools of SCET to construct a field theory description of the physics and build a framework that allows the small mass expansion to be studied systematically at higher orders.

2.1 Structure of the scalar integrals

Our analysis of the process begins by applying the MoR to individual scalar Feynman integrals. This procedure was carried out in detail in parameter space for one- and two-loop integrals in Ref. [92] and used to calculate the integrals in an expansion around a small quark mass. Here, we will repeat this procedure instead focusing on building an interpretation of each region in terms of the scaling of the loop-momentum.

To obtain the regions, we first express the integrals using the Lee-Pomeransky representation [93]. A scalar integral corresponding to a graph G in $D = 4 - 2\epsilon$ space-time dimensions may be written as,

$$\mathcal{I}(G) = \frac{\Gamma(D/2)}{\Gamma((L+1)D/2 - \nu) \prod_{e \in G} \Gamma(\nu_e)} \int_0^\infty \left(\prod_{e \in G} \frac{dx_e}{x_e} \right) I(\mathbf{x}; \mathbf{s}), \quad (2.10)$$

$$I(\mathbf{x}; \mathbf{s}) = \left(\prod_{e \in G} x_e^{\nu_e} \right) \cdot (\mathcal{P}(\mathbf{x}; \mathbf{s}))^{-D/2}, \quad \mathcal{P}(\mathbf{x}; \mathbf{s}) \equiv \mathcal{U}(\mathbf{x}) + \mathcal{F}(\mathbf{x}; \mathbf{s}), \quad (2.11)$$

where ν_e is the exponent of the denominator associated to the propagator e , and $\nu \equiv \sum_{e \in G} \nu_e$. The polynomial $\mathcal{P}(\mathbf{x}; \mathbf{s})$ is the Lee-Pomeransky polynomial, for an N propagator integral it depends on N Lee-Pomeransky parameters which we denote by \mathbf{x} and a set of Lorentz invariants (or Mandelstam variables) and masses which we denote collectively by \mathbf{s} . The polynomials $\mathcal{U}(\mathbf{x})$ and $\mathcal{F}(\mathbf{x}; \mathbf{s})$ are the first and second Symanzik polynomials.

The particular limit we are interested in can be defined by introducing a small parameter λ and rescaling the kinematic invariants/masses according to:

$$m_t \rightarrow \lambda m_t, \quad s \rightarrow s, \quad t \rightarrow t, \quad u \rightarrow u. \quad (2.12)$$

In parameter space, each region is defined as a set of scalings (with respect to the small parameter λ) of each Lee-Pomeransky parameter. For example, for an integral depending on the parameters x_1, \dots, x_N , a region (R) may be given by the scaling

$$(R) : \quad x_1 \rightarrow \lambda^{u_1^R} x_1, \quad x_2 \rightarrow \lambda^{u_2^R} x_2, \quad \dots, \quad x_N \rightarrow \lambda^{u_N^R} x_N, \quad (2.13)$$

along with an overall rescaling of the expansion parameter $\lambda \rightarrow \lambda^{u_{N+1}^R}$. The set of scalings can be collected into a region vector $\mathbf{u}^R = (u_1^R, \dots, u_{N+1}^R)$. For Euclidean kinematics, the regions that appear in parameter space can be obtained automatically using existing tools [94,95]². One advantage of using the Lee-Pomeransky representation for the MoR is that the scaling of parameter x_e is identical to the scaling of the corresponding propagator up to an overall shift of the \mathbf{u} vector [73,97].

In general, the expanded integrals are no longer regulated in dimensional regularisation. Instead, we find a new type of singularity that cancels between the different regions. These rapidity divergences are due to the so-called factorisation (or collinear) anomaly [98,99]. The physical reason for their appearance has been understood in SCET as a breakdown of the EFT's classical boost (or reparametrisation) symmetry by quantum corrections. We can regulate this type of singularity by using an analytic regulator, i.e. shifting the powers of the propagators away from 1 to $1 \pm \eta$. Once all regions are added, the procedure involves taking the limit $\eta \rightarrow 0$ *before* imposing the limit $\epsilon \rightarrow 0$ to obtain the correct answer.

2.1.1 One-loop

Let us consider the one-loop scalar box integral shown in Fig. 2, the integral is defined in momentum space as,

$$I = e^{\gamma_E \epsilon} \mu^{2\epsilon} \int \frac{d^D \ell}{i\pi^{D/2}} \frac{1}{[\ell^2 - m_t^2]^\alpha [(\ell + q_1)^2 - m_t^2]^\beta [(\ell + q_1 + q_2)^2 - m_t^2]^\gamma [(\ell - q_3)^2 - m_t^2]^\delta}. \quad (2.14)$$

Expanding around small m_t using the MoR, we obtain five regions in parameter space,

$$\mathbf{u}^{(1)} = (-2, -2, 0, 0), \quad \mathbf{u}^{(2)} = (0, -2, -2, 0), \quad \mathbf{u}^{(3)} = (-2, 0, 0, -2),$$

²It is known that, away from Euclidean kinematics additional work has to be done to reveal hidden/Glauber regions, see for example Refs. [74,94,96].

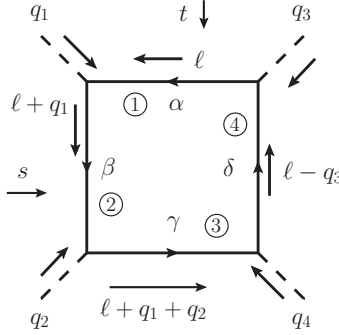


Figure 2: Kinematics of the one-loop scalar box integral. The internal lines are massive, with mass m_t , and the external lines are massless. The circled numbers refer to the order in which the propagators appear in the region vectors in (2.15) and $\alpha, \beta, \gamma, \delta$ refer to the propagator powers.

$$\mathbf{u}^{(4)} = (0, 0, -2, -2), \quad \mathbf{u}^{(5)} = (0, 0, 0, 0). \quad (2.15)$$

These regions correspond to the various internal propagators having either a hard scaling $\sim \lambda^0$ or a power suppressed scaling $\sim \lambda^2$. The regions are identical to those considered in Ref. [92] up to a rescaling required to convert the Lee-Pomeransky parameters to Feynman parameters, see Eq.(2.8) of Ref. [73].

While it is possible to calculate the integrals directly for each region, we would first like to interpret these regions in terms of the scaling of the loop-momentum ℓ . This will help us in Section 3, where we connect our calculation to SCET and derive a factorisation theorem.

Let us begin with the region $\mathbf{u}^{(1)}$. Based on the region vector, we can infer that the propagators $\ell^2 - m_t^2$ and $(\ell + q_1)^2 - m_t^2$ must scale as λ^2 and that $(\ell + q_1 + q_2)^2 - m_t^2$ and $(\ell - q_3)^2 - m_t^2$ scale as λ^0 . For energetic particles close to the mass shell, it is natural to formulate the analysis in terms of components of the momenta decomposed using light-cone vectors as follows

$$\ell^\mu = \underbrace{(n_+ \cdot \ell)}_{\ell_-^\mu} \frac{n_-^\mu}{2} + \underbrace{(n_- \cdot \ell)}_{\ell_+^\mu} \frac{n_+^\mu}{2} + \ell_\perp^\mu = (n_+ \cdot \ell, n_- \cdot \ell, \ell_\perp). \quad (2.16)$$

where n_-^μ and n_+^μ are the two light-like vectors satisfying $n_-^2 = n_+^2 = 0$, $n_- \cdot n_+ = 2$, and \perp indicates the directions perpendicular to both of these vectors. If we take the q_1^μ momentum to be in the n_-^μ direction, such that $n_+ \cdot q_1 \sim \lambda^0$, and consider our loop momentum to be collinear to q_1 , i.e.

$$\ell^\mu = \underbrace{(n_+ \cdot \ell)}_{\mathcal{O}(\lambda^0)} \frac{n_-^\mu}{2} + \underbrace{(n_- \cdot \ell)}_{\mathcal{O}(\lambda^2)} \frac{n_+^\mu}{2} + \underbrace{\ell_\perp^\mu}_{\mathcal{O}(\lambda)}, \quad (2.17)$$

we obtain the following scalings for the scalar products

$$\ell^2 \sim \lambda^2 Q^2, \quad \ell \cdot q_1 \sim \lambda^2 Q^2, \quad \ell \cdot q_2 \sim \lambda^0 Q^2, \quad \ell \cdot q_3 \sim \lambda^0 Q^2, \quad (2.18)$$

\mathbf{u}^R	order	interpretation	routing
(-2, -2, 0, 0)	$4 - 2(\epsilon + \alpha + \beta)$	c_1	ℓ
(0, -2, -2, 0)	$4 - 2(\epsilon + \beta + \gamma)$	c_2	$\ell - q_1$
(-2, 0, 0, -2)	$4 - 2(\epsilon + \alpha + \delta)$	c_3	$\ell + q_3$
(0, 0, -2, -2)	$4 - 2(\epsilon + \gamma + \delta)$	c_4	$\ell - q_1 - q_2$
(0, 0, 0, 0)	0	h	n/a

Table 1: The regions of the one-loop diagram and their interpretation in terms of hard and collinear modes. The routing is identified by specifying the momentum flowing through the propagator labelled α in Fig. 2. Note that for the scalar “corner” integral $\alpha = \beta = \gamma = \delta = 1$ and all regions enter at leading power.

since by construction there is a wide separation between the directions of the four external particles. Inputting these scalings into the propagators, we see that the region described by the region vector $\mathbf{u}^{(1)}$ is consistently identified as the one with loop momentum collinear to q_1 . We denote this region as c_1 .

To reveal the nature of the second region $\mathbf{u}^{(2)}$, we need to perform a shift in the loop momentum because, according to the region vector, the third propagator, namely $(\ell + q_1 + q_2)^2 - m_t^2$ in the original routing, should scale as λ^2 . However, despite the fact that $\ell \cdot q_2 \sim \lambda^2$, the propagator scales as λ^0 since $q_1 \cdot q_2 \sim \lambda^0$. As such, we note a well-known fact: the diagram’s momentum routing can obscure a region’s physical nature. In the region where the loop momentum ℓ is collinear to q_2 , the scalar products scale as

$$\ell^2 \sim \lambda^2 Q^2, \quad \ell \cdot q_1 \sim \lambda^0 Q^2, \quad \ell \cdot q_2 \sim \lambda^2 Q^2, \quad \ell \cdot q_3 \sim \lambda^0 Q^2, \quad (2.19)$$

and we find that the correct scaling for the propagators is obtained after shifting $\ell \rightarrow \ell - q_1$ in Fig. 2. With the correct routing, we can now identify the region described by region vector $\mathbf{u}^{(2)}$ as collinear to q_2 , i.e. c_2 .

Finally, to reveal $\mathbf{u}^{(3)}$ and $\mathbf{u}^{(4)}$ we must consider the frame spanned by q_3 and q_4 . It should not be surprising that our ability to identify regions depends on which of the four-momenta we eliminate or, in other words, which frame we choose. One can easily show that using the shifts $\ell \rightarrow \ell + q_3$ and $\ell \rightarrow \ell - q_1 - q_2$ we can identify the momentum-space representation for regions defined by vectors $\mathbf{u}^{(3)}$ and $\mathbf{u}^{(4)}$ respectively. The fifth region, $\mathbf{u}^{(5)}$, is easily identified as the hard region, which always manifests as $u_i^R = 0$. As all components of the loop momentum are large, it does not matter which frame or routing we consider.

We summarise our findings in Table 1. The order in λ at which each region begins contributing is shown in the second column. At the level of the scalar integral, in the limit $\epsilon \rightarrow 0$ and $\alpha, \beta, \gamma, \delta \rightarrow 1$, all regions enter and contribute at leading power $\sim \lambda^0$. In Fig. 3, we depict each region and their physical interpretation, propagators shown in **orange** are collinear to external momentum, while **black** propagators are hard modes.

Our choice of rapidity regulator makes the soft region scaleless at one-loop, but this is not true for a different choice of regulator. For example, by setting the analytic regulators

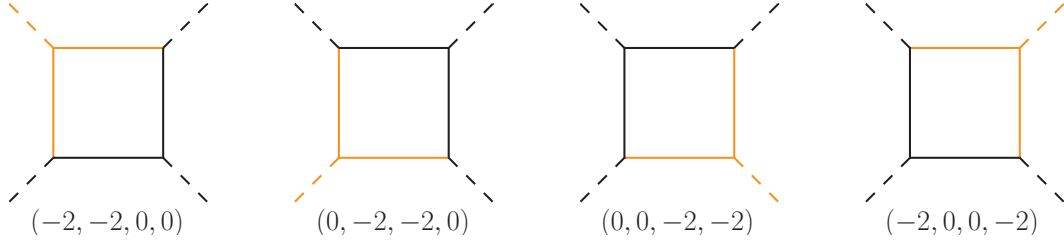


Figure 3: Regions for the one-loop diagram in Fig. 1. The **orange** propagators are collinear to one of the external momenta (also coloured), while the **black** propagators have a hard scaling. Purely hard region with all propagators **black** is not depicted.

$\alpha = \beta = \gamma = \delta = 1$ and instead introducing an additional propagator $1/(2\ell \cdot (q_2 - q_1))^n$ to regulate the integral, we obtain two additional regions,

$$\mathbf{u}^{(6)} = (-2, -1, 0, -1, -1), \quad \mathbf{u}^{(7)} = (0, -1, -2, -1, -1). \quad (2.20)$$

The new regions enter at leading power in λ for the scalar integrals and can be interpreted as soft regions. The loop momentum has the following scaling in the newly revealed soft regions,

$$\ell^\mu = \underbrace{(n_+ \cdot \ell)}_{\mathcal{O}(\lambda)} \frac{n_-^\mu}{2} + \underbrace{(n_- \cdot \ell)}_{\mathcal{O}(\lambda)} \frac{n_+^\mu}{2} + \underbrace{\ell_\perp^\mu}_{\mathcal{O}(\lambda)}, \quad (2.21)$$

yielding the following scaling for the scalar products

$$\ell^2 \sim \lambda^2 Q^2, \quad \ell \cdot q_1 \sim \lambda Q^2, \quad \ell \cdot q_2 \sim \lambda Q^2. \quad (2.22)$$

The particular choice of the regulator adopted here is consistent with Ref. [81] for on-shell kinematics and preserves the analytic properties of the integral.

Once the regions and routings which reveal their nature in momentum space have been identified, we can perform calculation of the integrals directly in momentum space. The integral required in the hard region corresponds to the integral in (2.14) with $m_t = 0$. It well-defined without analytic regulators, so $\alpha = \beta = \gamma = \delta = 1$, and it is known in literature. However, the collinear regions require a new integral to be considered, which we perform with arbitrary powers α , β , γ , and δ . As an example, we will discuss the c_1 region, which, in momentum space, takes the form

$$I = e^{\gamma E \epsilon} \mu^{2\epsilon} \int \frac{d^D \ell}{i\pi^{D/2}} \frac{1}{[\ell^2 - m_t^2]^\alpha [(\ell + q_{1-})^2 - m_t^2]^\beta [2(\ell + q_{1-}) \cdot q_{2+}]^\gamma [-2\ell \cdot q_{3+}]^\delta}. \quad (2.23)$$

From this we can infer that $I \propto (n_- \cdot q_3)^{-\delta} (n_- \cdot q_2)^{-\gamma}$. Since q_{1-}^μ is the only external vector in the n_-^μ direction, we can deduce

$$I = \left(- \underbrace{(n_+ \cdot q_1)(n_- \cdot q_3)}_t \right)^{-\delta} \left(- \underbrace{(n_+ \cdot q_1)(n_- \cdot q_2)}_s \right)^{-\gamma} \left(m_t^2 \right)^{D/2 - \alpha - \beta} I_0(\alpha, \beta, \gamma, \delta; D), \quad (2.24)$$

where we have found the dependence on m_t from dimensional analysis. The remaining integral I_0 is now a function of the powers of propagators and the space-time dimension. Explicit calculation shows that

$$I_0 = \left(e^{\gamma_E \epsilon} \mu^{2\epsilon} \right) (-1)^{\alpha+\beta+\gamma+\delta} \frac{\Gamma[-2 + \epsilon + \alpha + \beta] \Gamma[\alpha - \gamma] \Gamma[\beta - \delta]}{\Gamma[\beta] \Gamma[\alpha]} \frac{1}{\Gamma[\alpha + \beta - \delta - \gamma]}. \quad (2.25)$$

This result concludes our discussion of the one-loop box, all other box integrals appearing in the amplitude can be obtained from crossing the diagram in Fig. 2.

2.1.2 Two-loop

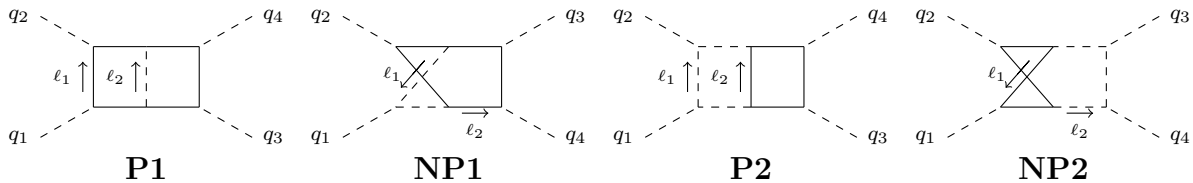


Figure 4: The four top-level two-loop topologies. Massless particles (Higgs bosons and gluons) are depicted with dashed lines, massive top quarks are shown as solid lines. We indicate the lines that carry the loop momenta for our default routing.

At the two-loop order, there are four top-level (7-propagator) topologies to consider, they are shown in Fig. 4: a planar box and a non-planar box that each contain either predominantly top quarks or gluon propagators. As the number of possible routings, frame choices, and regions proliferates beyond one-loop, we have automated the routing-finding algorithm. Our code considers the scaling of each scalar product for each possible region and frame and then applies it to all possible shifts. To limit the number of shifts, we only consider those that result in two propagators being directly identical to the two-loop momenta. We observe that this procedure is sufficient for the problem of identifying soft and collinear regions at hand, but it is possible to construct regions that cannot be straightforwardly revealed this way, for example Glauber, threshold and potential regions. This code is currently being integrated as part of pySecDec [100].

We begin by considering the diagram **P1**, shown in Fig. 4. We first use standard techniques to obtain the region vectors of expansion around small m_t in parameter space. In total, we obtain 13 regions for this diagram. In the limit $\epsilon \rightarrow 0$ we find that, for this planar scalar integral, all regions enter at leading power. Next, using the routing algorithm, we find a suitable routing that enables us to interpret the regions in terms of the scaling of the loop momenta. In Fig. 5 we display each region vector, using colours to represent the physical interpretation of each region, with **orange** for the first collinear mode, **blue** for the second collinear mode and **black** for hard modes. We note that all regions can be described purely in terms of the loop momenta becoming collinear to some external momenta. The soft mode is absent from the expansion of this diagram.

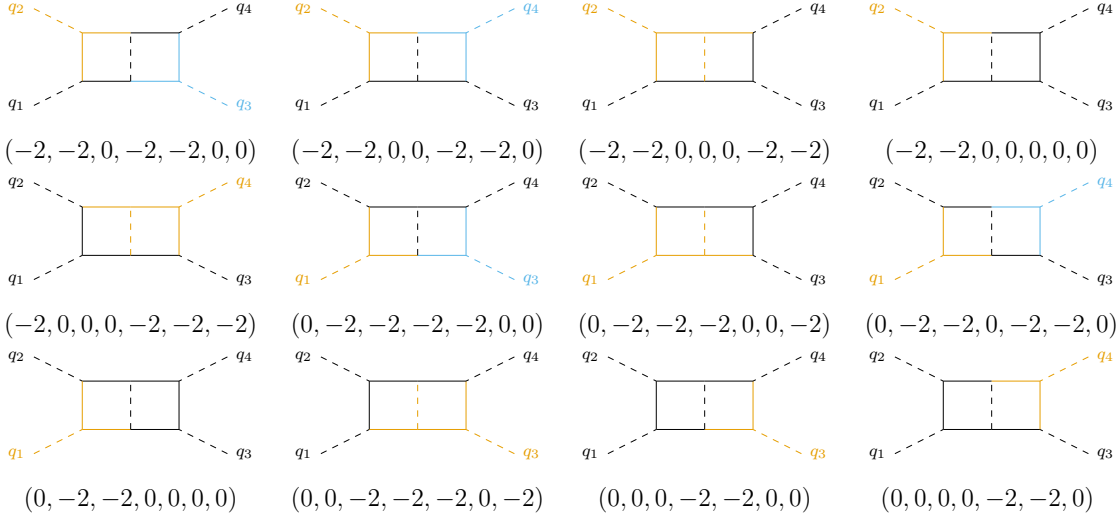


Figure 5: Regions for the two-loop diagram **P1** in Fig. 4. Propagators and external lines are coloured **orange** for the first collinear mode, **blue** for the second collinear mode, and **black** for the hard modes. Purely hard region is not depicted.

Next, we focus on the non-planar two-loop diagram **NP1**. Repeating the above procedure, we obtain 14 regions for this diagram. Here, we observe a new feature that was not present in the one-loop or two-loop planar diagrams: there is a mode that causes the propagators to scale as $\sim \lambda^1$. This new mode can be understood by allowing the loop momentum to have a soft scaling.

The interpretation of each region is again shown graphically in Fig. 6 with **orange** for the first collinear mode, **blue** for the second collinear mode, **green** for soft modes and **black** for hard modes. However, the presence of the soft region constrains the possible valid momentum routing further as it fixes the routing completely (up to permutations of ℓ_1 and ℓ_2). We also present the interpretations, along with shifts in routing needed to reveal the regions, in Table 2 for the convenience of the reader.

The region analysis of diagram **P2** and **NP2** proceeds similarly to **P1** and **NP1**, respectively. In all four topologies, all regions obtained can be interpreted as loop momenta becoming soft or collinear to an external momentum, see Appendix B for a depiction of each region and their interpretation in momentum space according to the colour coding described above.

In summary, we find that at the one- and two-loop level the following loop momenta modes are sufficient to interpret all regions appearing in the small-mass expansion,

$$\text{hard :} \quad \ell_H^\mu \sim Q(1, 1, 1), \quad (2.26)$$

$$\text{collinear} - q_i : \quad \ell_{C_i}^\mu \sim Q(1, \lambda^2, \lambda), \quad (2.27)$$

$$\text{soft :} \quad \ell_S^\mu \sim Q(\lambda, \lambda, \lambda). \quad (2.28)$$

For the collinear- q_i mode we use light-cone vectors n_+^μ and n_-^μ defined above generalised

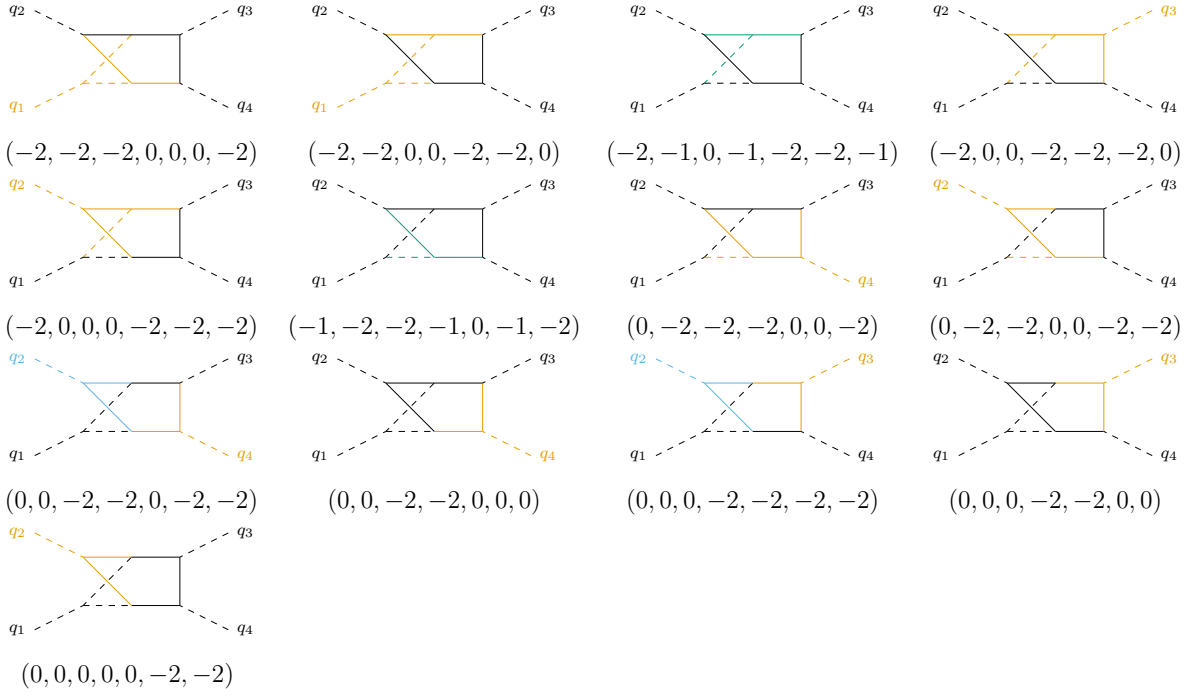


Figure 6: Regions for the two-loop diagram **NP1** in Fig. 4. Propagators and external lines are coloured **orange** for the first collinear mode, **blue** for the second collinear mode, **green** for the soft modes, and **black** for the hard modes. Purely hard region is not depicted.

\mathbf{u}^R	order	interpretation	routing
(-2, -2, -2, 0, 0, 0, -2)	-4ϵ	c_1c_1	ℓ_1, ℓ_2
(-2, -2, 0, 0, -2, -2, 0)	-4ϵ	c_1c_1	$\ell_1, \ell_2 - q_3 - q_4$
(-2, -1, 0, -1, -2, -2, -1)	$-1 - 4\epsilon$	ss	$\ell_1, \ell_2 - q_3 - q_4$
(-2, 0, 0, -2, -2, -2, 0)	-4ϵ	c_3c_3	$\ell_1, \ell_2 - q_4$
(-2, 0, 0, 0, -2, -2, -2)	-4ϵ	c_2c_2	$\ell_1, \ell_2 - q_3 - q_4$
(-1, -2, -2, -1, 0, -1, -2)	$-1 - 4\epsilon$	ss	$\ell_1 - q_1, \ell_2$
(0, -2, -2, -2, 0, 0, -2)	-4ϵ	c_4c_4	$\ell_1 - q_1, \ell_2$
(0, -2, -2, 0, 0, -2, -2)	-4ϵ	c_2c_2	$\ell_1 - q_1, \ell_2$
(0, 0, -2, -2, 0, -2, -2)	-4ϵ	$c_4\bar{c}_2$	$\ell_1 - \ell_2 + q_3 + q_4, \ell_1$
(0, 0, -2, -2, 0, 0, 0)	-2ϵ	c_4h	$\ell_1 - \ell_2 + q_3 + q_4, \ell_1$
(0, 0, 0, -2, -2, -2, -2)	-4ϵ	$c_3\bar{c}_2$	$\ell_1 - \ell_2 + q_3, \ell_1 - q_4$
(0, 0, 0, -2, -2, 0, 0)	-2ϵ	c_3h	$\ell_1 - \ell_2 + q_3, \ell_1 - q_4$
(0, 0, 0, 0, 0, -2, -2)	-2ϵ	hc_2	$\ell_1, \ell_1 + \ell_2 - q_3 - q_4$
(0, 0, 0, 0, 0, 0, 0)	0	hh	n/a

Table 2: The regions of the two-loop diagram **NP1** and their interpretation in terms of hard, collinear, and soft modes. The routing shifts are relative to one given for the **NP1** diagram in Fig. 4. The order given is valid when all propagators are raised to power 1 and the dependence on additional analytic regulators is suppressed.

for each of the collinear directions. See beginning of Section 3 for explicit construction.

2.1.3 Three-loop and beyond

In the previous sections, we have categorised the loop momenta scaling relevant for understanding the region expansion up to two-loops. The complete knowledge of these regions allows us to compute the one-loop and two-loop amplitudes not only at leading power but also at any order in the power expansion.

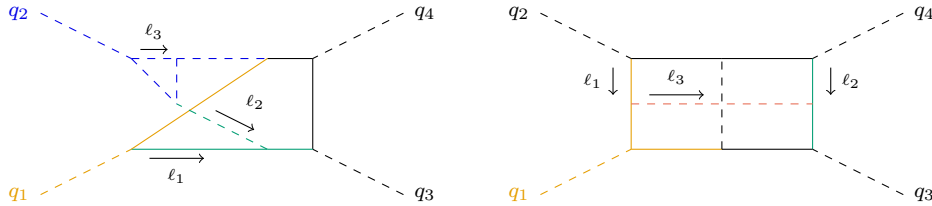


Figure 7: Example three-loop diagrams containing modes beyond soft, collinear, and hard. (left) A region with a hard-collinear- q_2 loop momentum, shown in **blue**. (right) A region containing a soft-collinear- q_1 loop momentum, shown in **pink**. Both diagrams also contain soft in **green** and collinear in **orange** loop momenta.

If we wish to understand the all-order structure of the QCD corrections to HH production at any order in the power expansion, we must ask if additional loop momenta scalings appear in the region expansion beyond two-loops. We generate all diagrams relevant to Higgs pair production at three-loops and obtain a list of all regions appearing in the MoR analysis for each diagram. Using the tool described in the previous section, we find that considering only the collinear and soft loop momenta modes is insufficient to capture the regions appearing at three-loops, see Figure 7 for example diagrams that contain additional loop momenta modes. However, adding the following three-loop momenta modes allows us to describe the regions appearing in diagrams containing up to three-loops,

$$\text{hard - collinear - } q_i : \quad \ell_{HC_i}^\mu \sim Q(1, \lambda, \lambda^{1/2}), \quad (2.29)$$

$$\text{soft - collinear - } q_i : \quad \ell_{SC_i}^\mu \sim Q(\lambda, \lambda^2, \lambda^{3/2}), \quad (2.30)$$

$$\text{ultra - soft :} \quad \ell_{US}^\mu \sim Q(\lambda^2, \lambda^2, \lambda^2). \quad (2.31)$$

The appearance of new loop momentum scalings at each loop order in the small mass expansion is consistent with other results in the literature, see for example Ref. [70], which discusses the modes appearing in the small mass expansion of heavy-to-light decays. In the present analysis, we expect further modes to enter at four-loop and for each additional loop order.

Suppose we instead only wish to understand the all-order structure at leading power. In that case, it is important to consider not only the regions relevant to the expansion of

the scalar integrals but also the order in which they are relevant to the power expansion of the complete amplitude. In particular, regions can be power-suppressed (or enhanced) by the non-trivial numerator structure of gauge amplitudes. In Sections 2.2 and 2.3 we will analyse the power suppression due to the numerator of the amplitude at one- and two-loops, respectively. In Section 3, we will discuss the general all-order structure of the amplitude.

2.2 Structure of the one-loop amplitude

The hard region can be computed by rescaling parameters according to Eq. (2.13) with region vector $\mathbf{u}^{(h)}$ and then expanding about small λ . This procedure is equivalent to *directly* expanding the original integrand in m_t . Expanding to next-to-leading power, the hard region result for the first form factor is given by,

$$\begin{aligned}
A_{1,y_t^2}^{(h)} = & \frac{4y_t^2}{s} \left\{ 2 - 2m_t^2 \left[-\frac{2}{\epsilon^2 s} - \frac{1}{\epsilon} \left(\frac{s^2 + 2tu}{stu} l_s + \frac{l_t}{u} + \frac{l_u}{t} \right) \right. \right. \\
& + \frac{-l_s^2 + 2l_t^2 + 2l_u^2}{s} + \frac{l_s l_t}{t} + \frac{l_s l_u}{u} + \frac{(t-u)^2 l_t l_u}{stu} \\
& \left. \left. - \left(\frac{2}{s} + \frac{1}{t} + \frac{1}{u} \right) l_s - \frac{t l_t}{su} - \frac{u l_u}{st} + \frac{60 + 13\pi^2}{6s} \right] + \mathcal{O}(m_t^4) \right\}, \quad (2.32)
\end{aligned}$$

where $l_x = \ln(-\mu^2/x)$. The hard region can be evaluated without an additional analytic regulator and does not generate logarithms involving the top-quark mass. The leading power term in the m_t expansion is finite in the $\epsilon \rightarrow 0$ limit and corresponds to the massless, $m_t = 0$, amplitude. The terms at next-to-leading power and beyond contain poles in ϵ that must be cancelled by the poles appearing in the collinear regions.

The collinear regions can be computed similarly after rescaling parameters according to the region vectors $\mathbf{u}^{(c_1)}, \dots, \mathbf{u}^{(c_4)}$. The singularities in the collinear regions are not fully regulated by ϵ alone. We introduce an additional analytic regulator η with $\alpha = \beta = 1 + \eta$ and $\gamma = \delta = 1 - \eta$. The singular dependence on the additional regulator will cancel among the collinear regions, and we can ultimately take the limit $\eta \rightarrow 0$ after summing the results for the collinear regions. Computing each region of the first form factor to next-to-leading power we obtain:

$$\begin{aligned}
A_{1,y_t^2}^{(c_1)} = & \frac{-4y_t^2 m_t^2 \mu^{2\epsilon} e^{\gamma_E \epsilon} \Gamma(2\eta)^2 \Gamma(\epsilon + 2\eta)}{s(stu)(1 - 2\eta - \epsilon)\Gamma(4\eta)\Gamma(1 + \eta)^2} \left(\frac{1}{m_t^2} \right)^{2\eta + \epsilon} \\
& \times \left\{ (-t)^\eta (-u)^\eta \left[s^2 (1 + 2\epsilon^2 - (2 + \eta)\epsilon) - 2\eta tu \right] \right. \\
& + (-s)^\eta (-t)^\eta \left[su (1 + 2\epsilon^2 - (2 + \eta)\epsilon) - tu(1 - 3\eta - (2 - 5\eta)\epsilon) \right] \\
& \left. + (-s)^\eta (-u)^\eta \left[st (1 + 2\epsilon^2 - (2 + \eta)\epsilon) - tu(1 - 3\eta - (2 - 5\eta)\epsilon) \right] \right\}, \quad (2.33)
\end{aligned}$$

$$\begin{aligned}
A_{1,y_t^2}^{(c_2)} &= \frac{-4y_t^2 m_t^2 e^{\gamma_E \epsilon} \Gamma(-2\eta)}{s(stu) \Gamma(-\eta)^2} \left(\frac{\mu^2}{m_t^2} \right)^\epsilon \\
&\quad \left\{ (m_t^2)^{2\eta} (-t)^{-\eta} (-u)^{-\eta} \frac{(s^2(1+2\epsilon^2 - (2-\eta)\epsilon) + 2\eta tu) \Gamma(\epsilon - 2\eta) \Gamma(-2\eta)}{\eta^2(1+2\eta - \epsilon) \Gamma(-4\eta)} \right. \\
&\quad \left. + \left[(-s)^{-\eta} (-u)^\eta + (-s)^{-\eta} (-t)^\eta \right] \frac{4tu \Gamma(2\eta) \Gamma(-\eta) \Gamma(1+\epsilon)}{\epsilon \Gamma(1+\eta)} \right\}, \tag{2.34}
\end{aligned}$$

$$\begin{aligned}
A_{1,y_t^2}^{(c_3)} &= \frac{-2y_t^2 m_t^2 e^{\gamma_E \epsilon} \Gamma(-2\eta)}{s(stu) \eta^2 \Gamma(-\eta)^2} \left(\frac{\mu^2}{m_t^2} \right)^\epsilon \left\{ (m_t^2)^{2\eta} (-s)^{-\eta} (-u)^{-\eta} \frac{t^2 \Gamma(-2\eta) \Gamma(\epsilon - 2\eta)}{s(1+2\eta - \epsilon)(1-4\eta) \Gamma(-4\eta)} \right. \\
&\quad \times \left[-2s(1-4\eta)(1 - (2-\eta)\epsilon + 2\epsilon^2) + u(4 - 5\eta - (4-8\eta)\epsilon + 4\eta^2) \right] \\
&\quad + (-t)^{-\eta} (-u)^\eta \frac{16tu}{\Gamma(\eta)} \Gamma(1-\eta) \Gamma(1+2\eta) \Gamma(\epsilon) + (-s)^\eta (-t)^{-\eta} \frac{4tu \Gamma(1-\eta) \Gamma(2\eta) \Gamma(\epsilon)}{s(1-\epsilon) \Gamma(\eta)} \\
&\quad \left. \times \left[s(2 - 9\eta + (2+8\eta)\epsilon - 4\epsilon^2) + t(4 - 9\eta - (4-8\eta)\epsilon) \right] \right\}, \tag{2.35}
\end{aligned}$$

$$\begin{aligned}
A_{1,y_t^2}^{(c_4)} &= \frac{-2y_t^2 m_t^2 e^{\gamma_E \epsilon} \Gamma(-2\eta)}{s(stu) \eta^2 \Gamma(-\eta)^2} \left(\frac{\mu^2}{m_t^2} \right)^\epsilon \left\{ (m_t^2)^{2\eta} (-s)^{-\eta} (-t)^{-\eta} \frac{u^2 \Gamma(-2\eta) \Gamma(\epsilon - 2\eta)}{s(1+2\eta - \epsilon)(1-4\eta) \Gamma(-4\eta)} \right. \\
&\quad \times \left[(-2s(1-4\eta)(1 - (2-\eta)\epsilon + 2\epsilon^2) + t(4 - 5\eta - (4-8\eta)\epsilon + 4\eta^2)) \right] \\
&\quad + (-t)^\eta (-u)^{-\eta} \frac{16tu}{\Gamma(\eta)} \Gamma(1-\eta) \Gamma(1+2\eta) \Gamma(\epsilon) + (-s)^\eta (-u)^{-\eta} \frac{4tu \Gamma(1-\eta) \Gamma(2\eta) \Gamma(\epsilon)}{s(1-\epsilon) \Gamma(\eta)} \\
&\quad \left. \times \left[s(2 - 9\eta + (2+8\eta)\epsilon - 4\epsilon^2) + u(4 - 9\eta - (4-8\eta)\epsilon) \right] \right\}. \tag{2.36}
\end{aligned}$$

Two features are immediately apparent: firstly, the leading power $y_t^2 m_t^0$ term is not present for the collinear regions, and so their contribution to the amplitude starts only at the next-to-leading power, secondly, the collinear regions can generate logarithms of m_t from $(1/m_t^2)^{2\eta+\epsilon}$ hitting poles in either η or ϵ . The second feature means that the logarithmic dependence on m_t beyond leading power is significantly more complicated and necessitates the study of the collinear regions at next-to-leading power.

Here, we have presented results only for the first form factor. The second form factor can be computed straightforwardly using the same techniques; the expressions are significantly longer, but, the collinear regions are again suppressed relative to the hard region.

As will become apparent in what follows, the collinear regions are suppressed relative to the hard region at the level of the amplitude due to helicity conservation. We note that,

as discussed in Section 2.1.1, all regions contribute at leading power in the limit $\epsilon, \eta \rightarrow 0$ for the scalar integrals. However, when considering a collinear region, at amplitude level we can see that we obtain an extra power of m_t^2 from the Dirac algebra. We will discuss the reason behind this power suppression of soft/collinear regions in Section 3.

2.3 Structure of the two-loop amplitude

In Section 2.2, it was shown by explicit calculation that at one-loop, the collinear regions are suppressed by two powers of m_t relative to the hard region and thus do not contribute at leading power. We stated that the origin of this suppression at the amplitude level is helicity conservation. We now examine to what extent the collinear and soft regions are suppressed relative to the hard region beyond one-loop. As a starting point, let us consider the top-level two-loop topologies shown in Fig. 4. In principle, we could compute each region's amplitude at the two-loop level. However, it is possible to show that the contributions must be suppressed by considering the behaviour of the numerator of the amplitude without computing the scalar integrals.

The analysis of the non-planar topologies is more involved than the planar topologies due to the presence of the soft regions. Here, we will present the analysis of the regions of diagram **NP1** in detail; the procedure for the remaining diagrams follows identically. Considering the first region given in Table 2, both loop momenta, ℓ_1, ℓ_2 , are collinear to the external momentum p_1 . Taking just the numerator of the diagram, we can shift the loop momenta according to the ‘‘routing’’ column of Table 2. Next, we can insert the following scalings of the loop momenta,

$$\ell_1^2 \sim \lambda^2 Q^2, \quad \ell_2^2 \sim \lambda^2 Q^2, \quad \ell_1 \cdot \ell_2 \sim \lambda^2 Q^2, \quad \ell_1 \cdot q_1 \sim \lambda^2 Q^2, \quad \ell_2 \cdot q_1 \sim \lambda^2 Q^2, \quad (2.37)$$

which follows from the fact that the loop momenta are both collinear to q_1 . Furthermore, to leading power, if the loop momenta are collinear to an external momentum, then we can additionally use that

$$\ell_1 \propto q_1, \quad \ell_2 \propto q_1. \quad (2.38)$$

Inserting these relations, we find that the numerator of the amplitude, after applying projectors and computing traces, scales as λ^2 and is suppressed by two powers of m_t relative to the hard region. Since the scalar integral contributes at m_t^0 for this region, we can conclude that the region is suppressed by at least two powers of m_t .

Let us now consider the third region of **NP1** given in Table 2. In this region both loop momenta are instead soft and therefore scale as,

$$\begin{aligned} \ell_1^2 &\sim \lambda^2 Q^2, & \ell_2^2 &\sim \lambda^2 Q^2, & \ell_1 \cdot \ell_2 &\sim \lambda^2 Q^2, \\ \ell_1 \cdot q_2 &\sim \lambda Q^2, & \ell_1 \cdot q_3 &\sim \lambda Q^2, & \ell_1 \cdot q_4 &\sim \lambda Q^2, \\ \ell_2 \cdot q_2 &\sim \lambda Q^2, & \ell_2 \cdot q_3 &\sim \lambda Q^2, & \ell_2 \cdot q_4 &\sim \lambda Q^2. \end{aligned} \quad (2.39)$$

Inserting these relations into the numerator of the amplitude, we again find that it scales as λ^2 . However, unlike the collinear and hard regions, the underlying scalar integral itself is *enhanced* by a power of m_t^{-1} as can be seen in the 3rd and 6th rows of the “order” column of Table 2. Therefore, from this analysis, we conclude that, at the level of individual diagram topologies, the soft-soft region is suppressed by at least one power of m_t relative to the hard region.

This exercise may be repeated for each diagram and region entering the two-loop amplitude. We have performed this procedure for each of the top-level two-loop diagrams and observe that the soft and collinear regions are indeed suppressed by at least one power of m_t relative to the hard. This is consistent with the result of Ref. [51] in which the leading term of the two-loop amplitude appears to originate solely from the hard region. The discussion above was focussed only on topologies that include one closed fermion loop. We have verified that the outcome does not change when considering the full set of diagrams. This is also true beyond the two-loop level.

We remark that the above analysis can also be carried out at one-loop, which makes it possible to establish that the collinear regions are suppressed without having to compute any integrals as we did in Section 2.2.

Finally, we note that the hard, collinear, and soft regions can be computed separately at two-loops. We have argued that only the hard region is required to describe the amplitude at leading power, but all modes will eventually contribute beyond leading power. In principle, the amplitude computation in a given region is simpler than computing the entire amplitude and then expanding. This is because the amplitude will depend non-trivially on fewer scales after applying the method of regions, which simplifies the evaluation of the master integrals and, naively, results in a simpler IBP reduction. However, the presence of the analytic regulator complicates matters. Some IBP codes, such as Kira [101], support analytic regulators, but the regulator still increases the complexity, acting like an additional scale or dimensional regulator. Luckily, one may use the factorising properties of the amplitude (see Section 3) and only calculate the regions that are required to obtain the two-loop contribution to a jet function. Crucially, this implies that we can ignore the mixed hard and collinear regions that arise from a one-loop times one-loop contribution, which usually have a more complicated kinematic dependence. For integrals where, as in Eq. (2.24), the scaling factorises, the IBP can be carried out without any scales, greatly simplifying the calculation. Finally, by first expanding we also avoid having to calculate integrals to a higher power in m_t than required.

3 All-order factorisation in Effective Field Theory

The high-energy structure of the amplitude can be captured using subleading power SCET formalism suitable for processes with multiple collinear directions. Building on the fixed-order MoR investigations in the preceding sections, we construct an effective field theory description, which formalises and elucidates our findings to all orders in perturbation theory. We explore the structure of factorisation to next-to-leading power

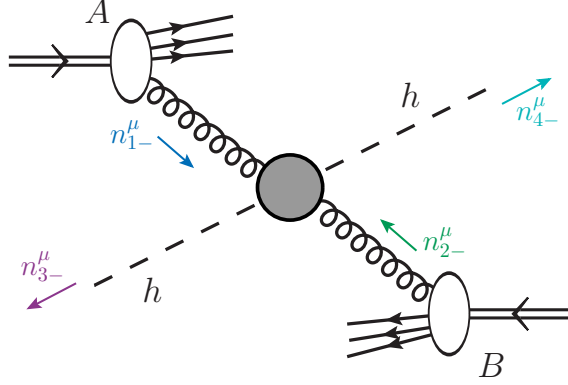


Figure 8: The light-cone directions for $gg \rightarrow HH$. In the partonic center-of-mass frame, the gluons and Higgs bosons are back-to-back; hence $n_{2\pm}$ can be eliminated in favour of $n_{1\mp}^\mu$, $n_{2\pm}^\mu = n_{1\mp}^\mu$ and similarly for $n_{4\pm}^\mu = n_{3\mp}^\mu$.

in the high-energy expansion where hard, collinear, and soft regions all contribute to the amplitude, and discuss the underlying reasons for the straightforward leading power result where only the hard region is present. In this section, we follow conventions introduced in [102–104], see also [105, 106].

To set up the framework, we generalise the notation introduced in the previous section and introduce a set of light-cone reference vectors n_{i-}^μ and n_{i+}^ν for each collinear direction i, j, \dots , such that $n_{i-} \cdot n_{j-} \sim n_{i+} \cdot n_{j+} \sim \mathcal{O}(1)$ for all $i \neq j \in \{1, 2, 3, 4\}$, and $n_{i+}^2 = n_{i-}^2 = 0$, $n_{i-} \cdot n_{i+} = 2$. In a generic reference frame, the on-shell external momenta for massless scattering can then be written as

$$q_i^\mu = (n_{i+} \cdot q_i) \frac{n_{i-}^\mu}{2}. \quad (3.1)$$

The metric tensor is decomposed as

$$g^{\mu\nu} = n_{i+}^\mu \frac{n_{i-}^\nu}{2} + n_{i-}^\mu \frac{n_{i+}^\nu}{2} + g_{\perp i}^{\mu\nu}, \quad (3.2)$$

which implicitly defines $g_{\perp i}^{\mu\nu}$, and for an arbitrary momentum k the decomposition along the i -th light-cone direction is given by

$$k^\mu = (n_{i+} \cdot k) \frac{n_{i-}^\mu}{2} + (n_{i-} \cdot k) \frac{n_{i+}^\mu}{2} + k_{\perp i}^\mu. \quad (3.3)$$

The label \perp_i denotes directions perpendicular to n_{i-}^μ and n_{i+}^μ such that $n_{i-} \cdot k_{\perp i} = n_{i+} \cdot k_{\perp i} = 0$, but not necessarily with respect to another direction j : $n_{i\pm} \cdot k_{\perp j} \neq 0$. For the 2-to-2 kinematics in the problem at hand, it is often convenient to use the partonic centre-of-mass frame, where $n_{1\pm}^\mu = n_{2\mp}^\mu$ and $n_{3\pm}^\mu = n_{4\mp}^\mu$.

3.1 Hard scale $\mu^2 \sim s$

The large kinematic invariants s, t, u for the wide-angle scattering amplitude set the hard scale for the process, at which the Standard Model has to be matched onto the effective field theory. The power-counting arguments given below are valid to all orders in the strong coupling constant α_s , and we work only to the leading order in the electroweak couplings. Nonetheless, we provide the relevant expression for the collinear Higgs Lagrangian below that can be used to extend this work to all orders in the electroweak expansion.

First, let us briefly review the SCET formalism for multi-jet processes. The SCET operators are constructed from collinear-gauge invariant building blocks given by [107],

$$\psi_{c_i}(x) \in \begin{cases} \chi_{c_i}(x) = W_{c_i}^\dagger(x) \xi_{c_i}(x) & i\text{-collinear quark,} \\ \mathcal{A}_{c_i \perp i}^\mu(x) = W_{c_i}^\dagger(x) [iD_{c_i \perp i}^\mu W_{c_i}(x)] & i\text{-collinear gluon,} \end{cases} \quad (3.4)$$

where $\xi_{c_i}(x)$ is the i -collinear quark field and the corresponding collinear covariant derivative is $iD_{c_i}^\mu(x) = i\partial^\mu + g_s A_{c_i}^\mu(x)$. The i -collinear Wilson line is defined as,

$$W_{c_i}(x) = \mathbf{P} \exp \left[ig_s \int_{-\infty}^0 ds n_{i+} \cdot A_{c_i}(x + sn_{i+}) \right], \quad (3.5)$$

where \mathbf{P} denotes the path ordering operator. A generic N -jet operator, up to relative $\mathcal{O}(\lambda^2)$ power-corrections, has the following structure [102],

$$J = \int \left[\prod_{ik} dt_{i_k} \right] C(\{t_{i_k}\}) \prod_{i=1}^N J_{c_i}(t_{i_1}, t_{i_2} \dots), \quad (3.6)$$

where $C(\{t_{i_k}\})$ is a generalised Wilson coefficient, depending on the complete set $\{t_{i_k}\} = \{t_{i_k} : i \in \{1, \dots, N\} \wedge k \in \{1, \dots, N_i\}\}$ of light-cone positions, that captures the hard modes and J_{c_i} is a product of N_i collinear building blocks associated with a specific collinear direction n_{i+}^μ ,

$$J_{c_i}(t_{i_1}, t_{i_2} \dots) = \prod_{k=1}^{N_i \leq 3} \psi_{c_{i_k}}(t_{i_k} n_{i+}). \quad (3.7)$$

Since the collinear particles have large momenta components of the order of the hard scale, the operators are non-local along the light-cone directions as indicated by the position variable t_{i_k} .

In SCET, every field has a unique scaling in the expansion parameter λ . Thus, analysing operators and their λ suppression is straightforward. A single building block is present at leading power in each collinear direction. There are three ways to extend the basis of operators to subleading powers [90, 102]. First, we can introduce ∂_\perp^μ derivatives, which act on the building blocks present already in the leading power configuration,

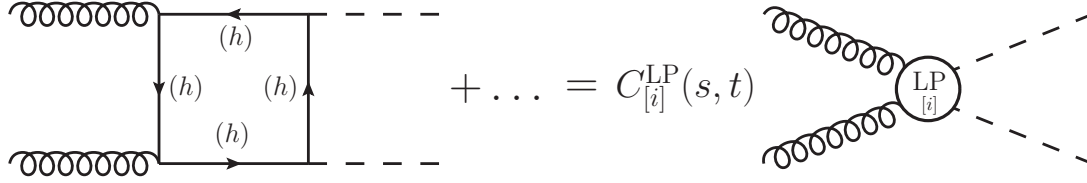


Figure 9: Graphical representation of the leading order matching to SCET at leading power. The label (h) denotes the hard scaling of the propagator. The ellipses indicate the remaining five box diagrams, namely the t - and u -type topologies, in addition to the depicted s -type topology, as well as the corresponding diagrams with reversed fermion flow of the top quark loop.

bringing an $\mathcal{O}(\lambda)$ suppression. Second, more building blocks can be added within each collinear direction. Each additional insertion of ψ_{c_i} induces an $\mathcal{O}(\lambda)$ suppression. Third, power suppression is induced by direct insertions of factors of m_t , which is treated as a building block to maintain homogeneous power-counting; see also [90]. The basis of sub-leading power currents includes time-ordered products of subleading power Lagrangian terms with lower power currents.

3.1.1 Leading power matching

In the case under consideration, the number of collinear directions is set to $N = 4$ and up to the two possible helicity projections³, there exists a unique field structure of leading power operators constructed from collinear gluon and Higgs fields,

$$J_{\text{LP}}^{[i]}(t_1, t_2, t_3, t_4) = y_t^2 \mathcal{P}_{[i]}^{\mu\nu} \mathcal{A}_{c_1 \perp 1 \mu}(t_1 n_{1+}) \mathcal{A}_{c_2 \perp 2 \nu}(t_2 n_{2+}) h_{c_3}(t_3 n_{3+}) h_{c_4}(t_4 n_{4+}), \quad (3.8)$$

with $i = 1, 2$ and the tensors $\mathcal{P}_{[i]}^{\mu\nu}$ are,

$$\mathcal{P}_{[1]}^{\mu\nu} = g^{\mu\nu} - \frac{n_{1-}^\nu n_{2-}^\mu}{n_{1-} \cdot n_{2-}}, \quad (3.9)$$

$$\mathcal{P}_{[2]}^{\mu\nu} = g^{\mu\nu} + \frac{n_{1-} \cdot n_{2-}}{n_{1-} \cdot n_{3-}} \frac{n_{3-}^\nu n_{3-}^\mu}{n_{2-} \cdot n_{3-}} - \frac{n_{1-}^\nu n_{3-}^\mu}{n_{1-} \cdot n_{3-}} - \frac{n_{3-}^\nu n_{2-}^\mu}{n_{3-} \cdot n_{2-}}. \quad (3.10)$$

To perform the matching as depicted in Fig. 9, we calculate in six-flavour QCD the following matrix element of the operators defined above,

$$\langle H(q_3) H(q_4) | \int dt \frac{1}{g_s^2} C_{[i]}^{\text{LP}}(t_1, t_2, t_3, t_4) J_{\text{LP}}^{[i]}(t_1, t_2, t_3, t_4) | g(q_1) g(q_2) \rangle \equiv A_{i, y_t^2}(s, t) \Big|_{\text{hard}} \quad (3.11)$$

where $d\mathbf{t} = dt_1 dt_2 dt_3 dt_4$. The form factor A_{i, y_t^2} was defined in (2.2). Here all particles are massless, i.e. only the hard region contributes to this matching as discussed in

³We could construct the alternative version of the basis using helicity building blocks as in [105, 106]. These two methods are equivalent except for the definition of evanescent operators.

Section 2.1. We could, in principle, perform this matching step in the unbroken phase of the Standard Model, but it does not offer any advantage when focusing only on the QCD corrections.

It is customary to define the Fourier-transformed Wilson coefficients,

$$C_{[i]}^{\text{LP}}(n_{1+} \cdot q_1, n_{2+} \cdot q_2, n_{3+} \cdot q_3, n_{4+} \cdot q_4) = \int dt_1 dt_2 dt_3 dt_4 C_{[i]}^{\text{LP}}(t_1, t_2, t_3, t_4) \quad (3.12)$$

$$\times e^{-i(n_{1+} \cdot q_1) t_1} e^{-i(n_{2+} \cdot q_2) t_2} e^{-i(n_{3+} \cdot q_3) t_3} e^{-i(n_{4+} \cdot q_4) t_4} ,$$

which depend on the large momentum components of all the collinear fields. Their respective arguments represent quantities in coordinate space and their Fourier-transformed counterparts. To shorten the notation, using reparametrisation invariance, we can trade the large momentum components for Mandelstam variables in the massless kinematics

$$C_{[i]}^{\text{LP}}(n_{1+} \cdot q_1, n_{2+} \cdot q_2, n_{3+} \cdot q_3, n_{4+} \cdot q_4) \equiv C_{[i]}^{\text{LP}}(s, t) , \quad (3.13)$$

with $s = 2q_1 \cdot q_2 = \frac{n_{1+} \cdot n_{2+}}{2} (n_{1+} \cdot q_1)(n_{2+} \cdot q_2)$, and $t = 2q_1 \cdot q_3 = \frac{n_{1+} \cdot n_{3+}}{2} (n_{1+} \cdot q_1)(n_{3+} \cdot q_3)$.

In addition to the leading power current given in (3.8), we will also require LP type currents with a single (anti)quark field building block in one or two of the collinear directions, $\chi_{c_i}(x)$ in (3.4). These currents can enter the description of the $gg \rightarrow HH$ amplitude through time-ordered products with subleading power Lagrangian terms, see the construction in [102]. In particular, through interactions with the $\mathcal{L}_{\xi q}$ Lagrangian an incoming collinear gluon can be turned into a collinear-quark soft-antiquark pair, the first of which can then participate in the hard scattering described by a current of the form:

$$J_{\text{LP}}(t_1, t_2, t_3, t_4) = y_t^2 \bar{\chi}_{c_1}(t_1 n_{1+}) \chi_{c_2}(t_2 n_{2+}) h_{c_3}(t_3 n_{3+}) h_{c_4}(t_4 n_{4+}) . \quad (3.14)$$

We discuss the role of these types of currents further in Section 3.2.

3.1.2 Next-to-leading power matching

We are now ready to discuss the leading power m_t dependence of the amplitude. Still, before we proceed, it is instructive to sketch the factorisation at next-to-leading power in m_t expansion to explain the origin of power suppression at NLO and NNLO for collinear regions observed in Section 2 and generalise it to all orders in α_s .

At next-to-leading power, several power-suppressed operators contribute. As outlined below Eq. (3.7), the basis is constructed from the basic building blocks considered in [102] and explicit insertions of m_t , in analogy with [90]. This section gives examples of two operators that appear already at leading order in α_s and are relevant for the leading logarithmic resummation at NLP.

The matching of the $gg \rightarrow HH$ amplitude to a subleading power SCET operator is presented graphically in Fig. 10. Besides trivial operators with explicit mass suppression, which are directly related to the leading power operator $J_{\text{NLP}}^{[i]}(t_1, t_2, t_3, t_4) =$

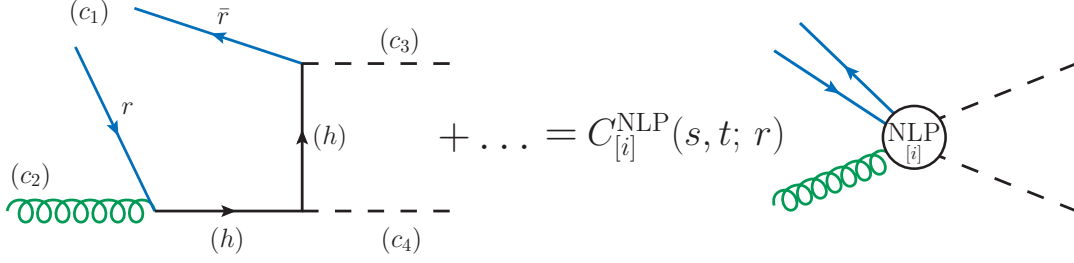


Figure 10: Matching to SCET at next-to-leading power. The (h) , (c_i) labels depict the scaling of each line. The fraction of collinear momentum carried by the (anti)quark in the (c_1) sector is denoted by $r(\bar{r})$, where $\bar{r} = (1 - r)$. The ellipses contain the remaining five permutations of the possible attachments.

$m_t^2 J_{\text{LP}}^{[i]}(t_1, t_2, t_3, t_4)$, we need to consider operators with two collinear quark fields in a single collinear direction.

We begin the analysis with the expression for the tree-level QCD process $t(q) + \bar{t}(q') + g(q_2) \rightarrow h(q_3) + h(q_4)$, with $q + q' = q_1$, depicted on the left-hand side. The full QCD expression for the drawn diagram reads,

$$\mathcal{M}_{\text{Fig10}}^{\text{QCD}} = \bar{v}(q') \left[\frac{-iy_t}{\sqrt{2}} \right]^2 \frac{i(-\not{q}' - \not{q}_3 + m_t)}{(q' + q_3)^2 - m_t^2} \frac{i(\not{q} + \not{q}_2 + m_t)}{(q + q_2)^2 - m_t^2} i g_s \mathbf{T}^B \gamma_\nu u(q) \varepsilon^\nu(q_2). \quad (3.15)$$

The matching is performed on-shell, i.e. the external gluon is chosen to be transverse, and spinors obey the Dirac equation $\not{q}u(q) = m_t u(q)$, $\bar{v}(q')\not{q}' = -\bar{v}(q')m_t$. Next, we expand the amplitude in m_t . The QCD spinor can be expanded according to (A.5), and all the momenta respect their collinear scaling. We also introduce momentum fraction r , such that $n_{1+} \cdot q = r n_{1+} \cdot q_1$ and $n_{1+} \cdot q' = \bar{r} n_{1+} \cdot q_1$, where $\bar{r} = (1 - r)$. The leading term in m_t is

$$\mathcal{M}_{\text{Fig10-LP}}^{\text{QCD}} = -i g_s \mathbf{T}^B \frac{y_t^2}{2} \frac{\varepsilon_{\perp 2}^\nu(q_2) \bar{v}_{c_1}(\bar{r}q_1) \not{n}_{3-}}{\bar{r}(n_{1+} \cdot q_1) n_{1-} \cdot n_{3-}} \frac{[2r(n_{1+} \cdot q_1) n_{1-\nu} + (n_{2+} \cdot q_2) \not{n}_{2-} \gamma_\nu]}{r(n_{1+} \cdot q_1)(n_{2+} \cdot q_2) n_{1-} \cdot n_{2-}} u_{c_1}(r q_1). \quad (3.16)$$

For the matching calculation, it is convenient to choose a frame where q_1 and q_2 are back-to-back, such that $n_{1\pm}^\mu = n_{2\mp}^\mu$ and $\perp_1 = \perp_2$ is perpendicular to the directions $n_{1\pm}^\mu$. With this choice, $\not{n}_{3-} \rightarrow n_{3-} \cdot \gamma_{\perp 1}$ since the contributions proportional to $\not{n}_{1\pm}$ vanish when acting on the collinear spinors. Thus, the results read

$$\mathcal{M}_{\text{Fig10-LP}}^{\text{QCD}} = -i g_s \mathbf{T}^B \frac{y_t^2}{2} \frac{\bar{v}_{c_1}(\bar{r}q_1) n_{3-} \cdot \gamma_{\perp 1}}{\bar{r}(n_{1+} \cdot q_1) n_{1-} \cdot n_{3-}} \frac{\not{n}_{1+} \gamma_{\perp 1 \nu} u_{c_1}(r q_1)}{2r(n_{1+} \cdot q_1)} \varepsilon_{\perp 1}^\nu(q_2). \quad (3.17)$$

We can further use the identity

$$\gamma_{\perp}^\mu \gamma_{\perp}^\nu \not{n}_{\pm} = (g_{\perp}^{\mu\nu} \mp i \epsilon_{\perp}^{\mu\nu} \gamma_5) \not{n}_{\pm}, \quad \text{where} \quad \epsilon_{\perp}^{\mu\nu} = \frac{1}{2} \epsilon^{\mu\nu\alpha\beta} n_{+\alpha} n_{-\beta}, \quad (3.18)$$

with the convention $\epsilon^{0123} = +1$. Eq. (3.17) then reduces to,

$$\mathcal{M}_{\text{Fig10-LP}}^{\text{QCD}} = \frac{ig_s \mathbf{T}^B}{n_{1-} \cdot n_{3-}} \frac{y_t^2}{2(n_{1+} \cdot q_1)^2} \frac{1}{r\bar{r}} \left(\bar{v}_{c_1}(\bar{r}q_1) \frac{\not{h}_{1+}}{2} u_{c_1}(rq_1) n_{3-\nu} \epsilon_{\perp 1}^\nu(q_2) \right. \\ \left. + \bar{v}_{c_1}(\bar{r}q_1) \frac{\not{h}_{1+}}{2} \gamma_5 u_{c_1}(rq_1) n_{3-}^\mu i\epsilon_{\mu\nu}^{\perp 1} \epsilon_{\perp 1}^\nu(q_2) \right), \quad (3.19)$$

where the result transforms as a scalar and pseudoscalar under rotations in the transverse plane in the first and second lines, respectively.

The most general basis for an operator built of two collinear fermions consists of scalar $\frac{\not{h}_{i+}}{2}$, pseudoscalar $\frac{\not{h}_{i+}}{2} \gamma_5$, and vector $\frac{\not{h}_{i+}}{2} \gamma_{\perp i}^\mu$ Dirac structures⁴. Concretely, the relevant operators are given by

$$J_{S_i}(t_{i_1}, t_{i_2}) = \bar{\chi}_{c_i}(t_{i_2} n_{i+}) \frac{\not{h}_{i+}}{2} \chi_{c_i}(t_{i_1} n_{i+}), \quad (3.20)$$

$$J_{P_i}(t_{i_1}, t_{i_2}) = \bar{\chi}_{c_i}(t_{i_2} n_{i+}) \frac{\not{h}_{i+}}{2} \gamma_5 \chi_{c_i}(t_{i_1} n_{i+}), \quad (3.21)$$

$$J_{V_i}^{\nu A}(t_{i_1}, t_{i_2}) = \bar{\chi}_{c_i}(t_{i_2} n_{i+}) \frac{\not{h}_{i+}}{2} \gamma_{\perp i}^\nu \mathbf{T}^A \chi_{c_i}(t_{i_1} n_{i+}). \quad (3.22)$$

Here, we write only colour singlet operators for scalar and pseudoscalars and colour octet for vector operators since only these operators contribute to the matrix element we consider. The Fourier transformation with respect to the positions t_{i_k} is defined by

$$J_{X_i}(n_{i+} \cdot q_i, r, \bar{r}) = (n_{i+} \cdot q_i)^2 \int dt_{i_1} dt_{i_2} e^{i(t_{i_1} r + t_{i_2} \bar{r}) n_{i+} \cdot q_i} J_{X_i}(t_{i_1}, t_{i_2}) \quad (3.23)$$

for $X = S, P, V$. Only the vector operator has a non-zero overlap with the gluon matrix element, while the scalar and pseudo-scalar operators do not contribute

$$\langle 0 | J_{S,P}(r) | g(q_1) \rangle = 0. \quad (3.24)$$

Since only scalar and pseudoscalar structures are present in the result in Eq. (3.19), the leading term in m_t expansion does not contribute to vector operators. Therefore, it does not mix with the gluon; see Fig. 11. *This result holds to all orders in α_s , since helicity is conserved in the limit $m_t \rightarrow 0$.* Moreover, summing all leading order diagrams, denoted by ellipses in Fig. 10, yields a vanishing result.

To get a non-zero contribution, we consider the subleading term in m_t in Eq. (3.15). The result reads

$$\mathcal{M}_{\text{Fig10NLP}}^{\text{QCD}} = ig_s \mathbf{T}^B \frac{y_t^2}{2(n_{1+} \cdot q_1)^2} \frac{1}{\bar{r}^2 r^2} \bar{v}_{c_1}(q') \frac{(2m_t)}{n_{1+} \cdot q_1} \frac{n_{4-}^\mu}{n_{1-} \cdot n_{4-}} \frac{n_{3-}^\eta}{n_{1-} \cdot n_{3-}} \frac{\not{h}_{1+}}{2}$$

⁴Scalar, pseudoscalar, and vector refer to transformation properties under rotations in the transverse plane.



Figure 11: Mixing of the subleading power collinear quark-antiquark operators with a collinear gluon (left) and Higgs (right). The mixing is forbidden for leading power scalar and pseudoscalar operators in the gluon case and vector operators in the Higgs case, to all orders in perturbation theory due to helicity conservation in the massless limit.

$$\times \left[g_{\perp 1 \mu \nu} \gamma_{\perp 1 \eta} - g_{\perp 1 \mu \eta} \gamma_{\perp 1 \nu} + g_{\perp 1 \nu \eta} \gamma_{\perp 1 \mu} \right] u_{c_1}(q) \varepsilon'_{\perp 1}(q_2) \quad (3.25)$$

This time, we obtain non-zero matching onto the vector operator. Consequently, this structure can contribute to the amplitude at all orders starting from subleading power in the λ expansion, as explicitly demonstrated in Section 2.

On the effective field theory side, the structure encountered in the above calculation is naturally reproduced by the next-to-leading power operator of the following form

$$J_{\text{NLP}}^{[1]}(t_1, t_2, t_3, t_4) = y_t^2 m_t J_{V_1}^{\nu A}(t_1, t_2) \mathcal{A}_{\nu}^{c_2 \perp 2 A}(t_2 n_{2+}) h_{c_3}(t_3 n_{3+}) h_{c_4}(t_4 n_{4+}), \quad (3.26)$$

where an additional collinear field generates power suppression in one collinear direction and the m_t insertion. To avoid cumbersome notation in the example, we have dropped the projection operators introduced in Eq. (3.9). However, these can be reinstated to obtain the two scalar amplitude structures defined in (2.2). The matching coefficient $C_{[i]}^{\text{NLP}}(s, t; r)$ is extracted by considering a matrix element of the operator similarly to the leading power case in Eq. (3.11), now with an incoming collinear quark-antiquark pair instead of one of the gluons, and comparing with results in Eq. (3.25). For the first projection operator, which ultimately corresponds to the $g_{\perp}^{\mu\nu}$ structure, we find

$$C_{[1]}^{\text{NLP}}(s, t; r) = -\frac{1}{2(n_{1+} \cdot q_1)^2} \frac{1}{\bar{r}^2 r^2} \frac{2g_{\perp 1 \mu \nu}}{n_{1+} \cdot q_1} \frac{n_{4-}^{\mu}}{n_{1-} \cdot n_{4-}} \frac{n_{3-}^{\nu}}{n_{1-} \cdot n_{3-}}. \quad (3.27)$$

We point out that the endpoint divergences present in the matching coefficient as $\bar{r}, r \rightarrow 0$ must be dealt with before consistent NLP resummation can be achieved. Single power endpoint divergences have previously been observed in [81, 108–110]. Here, the additional momentum fractions arise from the power-suppressed parts of the collinear spinors and hence are constrained by reparametrisation invariance [104].

Identical considerations follow for the calculation of the matching coefficient of the next-to-leading power operator contributing in the sector collinear to the second gluon, which is given by

$$J_{\text{NLP}}^{[2]}(t_1, t_2, t_3, t_4) = y_t^2 m_t \mathcal{A}_{\nu}^{c_1 \perp 1 A}(t_1 n_{1+}) J_{V_2}^{\nu A}(t_2, t_2) h_{c_3}(t_3 n_{3+}) h_{c_4}(t_4 n_{4+}). \quad (3.28)$$

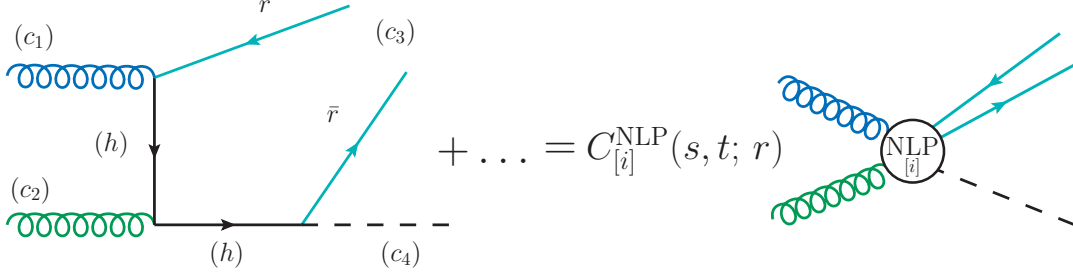


Figure 12: Matching to SCET at next-to-leading power. The (h) , (c_i) labels depict the scaling of each line. The fraction of collinear momentum carried by the (anti)quark in the (c_3) sector is denoted by $r(\bar{r})$, where $\bar{r} = (1 - r)$. The ellipses contain the remaining five permutations of the possible attachments.

However, as our second concrete example, we focus on the structure of contributions in the collinear direction defined by one of the final state Higgs bosons. The graphical matching equation analogous to one appearing in Fig. 10 is depicted in Fig. 12. Starting from the full QCD amplitude for the diagram present on the left-hand side, we perform the expansion in m_t and find the following leading power result

$$\begin{aligned}
\mathcal{M}_{\text{Fig12-LP}}^{\text{QCD}} &= ig_s^2 \mathbf{T}^B \mathbf{T}^A \frac{y_t}{\sqrt{2}} \bar{v}_{c_3}(q') \frac{1}{\bar{r}(n_{3+q_3})} \left[\frac{2n_{3-\mu}}{(n_{1+q_1})n_{3-} \cdot n_{1-}} \frac{\not{h}_{3+}}{2} \gamma_{\nu\perp 3} u_{c_3}(q) \right. \\
&+ \frac{1}{r(n_{3+q_3})n_{3-} \cdot n_{1-}} \left(n_{1-} \cdot n_{3-} n_{3+\nu} \frac{\not{h}_{3+}}{2} \gamma_{\mu\perp 3} u_{c_3}(q) - n_{3+\nu} n_{3-\mu} \frac{\not{h}_{3+}}{2} n_{1-} \cdot \gamma_{\perp 3} u_{c_3}(q) \right. \\
&\left. \left. + n_{1-} \cdot n_{3+} n_{3-\mu} \frac{\not{h}_{3+}}{2} \gamma_{\nu\perp 3} u_{c_3}(q) + \frac{\not{h}_{3+}}{2} \gamma_{\nu\perp 3} n_{1-} \cdot \gamma_{\perp 3} \gamma_{\mu\perp 3} u_{c_3}(q) \right) \right] \varepsilon_{\perp 2}^\nu(q_2) \varepsilon_{\perp 1}^\mu(q_1) \quad (3.29)
\end{aligned}$$

We note that the leading power result here exhibits the vector structure in contrast to the leading power result found in the c_1 sector in Eq. (3.19). Nonetheless, this structure cannot contribute to the amplitude since here, the mixing has to occur with the Higgs boson, which has a vanishing overlap

$$\langle h(q_3) | J_V^\mu(r) | 0 \rangle = 0. \quad (3.30)$$

To arrive at a non-vanishing contribution, we consider the subleading term in m_t to the QCD diagram in Fig. 12. The resulting expression is a few lines long and it is not enlightening to express here. It suffices to note that the structure in the transverse spin plane is scalar and pseudoscalar, as expected. Therefore, the operator which takes part in this matching is given by

$$J_{\text{NLP}}^{[3]}(t_1, t_2, t_{3_1}, t_{3_2}, t_4) = y_t m_t \mathcal{A}_\nu^{c_1\perp 1 A}(t_1 n_{1+}) \mathcal{A}_{c_2\perp 2}^{\nu A}(t_2 n_{2+}) J_{S_3}(t_{3_1}, t_{3_2}) h_{c_4}(t_4 n_{4+}), \quad (3.31)$$

where the m_t power suppression is generated by the two collinear quark fields in the c_3 direction. It is also noteworthy that this operator contains one less explicit power of y_t

than the leading power operator since there is one less Higgs field present. This factor is compensated at the level of the NLP matrix element by the collinear quark-antiquark-Higgs interaction vertex since it is required to have an external Higgs present, see the explicit result in Eq. (3.43). The analogous operator is needed for the case where power suppression is generated by the collinear quark and antiquark fields in the c_4 sector

$$J_{\text{NLP}}^{[4]}(t_1, t_2, t_3, t_{4_1}, t_{4_2}) = y_t m_t \mathcal{A}_\nu^{c_1 \perp_1 A}(t_1 n_{1+}) \mathcal{A}_{c_2 \perp_2}^{\nu A}(t_2 n_{2+}) h_{c_3}(t_3 n_{3+}) J_{S_4}(t_{4_1}, t_{4_2}). \quad (3.32)$$

3.2 Scale $\mu^2 \sim m_t^2$

At the scale parametrically of the order of m_t , we evaluate matrix elements of the operators in equations (3.8), (3.26), (3.28), (3.31), and (3.32) in SCET_{II}. Here, the top-quark mass is considered heavy, and we must consistently perform matching on a theory with the relevant low-energy degrees of freedom, which is carried out in Section 3.2.1 and Section 3.2.2. First, we recall the leading power collinear Lagrangian for massive fermions [66, 111]

$$\mathcal{L}_{c_i}^{(0)} = \bar{\xi}_{c_i} \left[i n_{i-} \cdot D_{c_i} + \left(i \not{D}_{c_i \perp_i} - m_q \right) \frac{1}{i n_{i+} \cdot D_{c_i}} \left(i \not{D}_{c_i \perp_i} + m_q \right) \right] \frac{\not{n}_{i+}}{2} \xi_{c_i}, \quad (3.33)$$

where, unlike in the SCET_I Lagrangian, the covariant derivative does not contain a soft gauge field

$$i D_{c_i}^\mu(x) = i \partial^\mu + g_s A_{c_i}^\mu(x). \quad (3.34)$$

In addition, we need the collinear Higgs Lagrangian. Since we work to the leading order in the electroweak parameters, only a single insertion of this Lagrangian is required for the NLP matrix elements. The collinear Higgs fields scale as $h_{c_i} \sim \lambda$, $i = 3, 4$, and the Lagrangian reads

$$\begin{aligned} \mathcal{L}_h^{(0)} = & \sum_{i=3,4} \left[\frac{1}{2} \left(n_{i+} \cdot \partial h_{c_i} n_{i-} \cdot \partial h_{c_i} + \partial_\mu^\perp h_{c_i} \partial_{\perp_i}^\mu h_{c_i} - m_h^2 h_{c_i}^2 \right) - \frac{g}{2m_W} \frac{m_h^2}{2} h_{c_i}^3 \right. \\ & \left. - \left(\frac{g}{2m_W} \right)^2 \frac{m_h^2}{8} h_{c_i}^4 - \left(\sum_q^{n_f} \frac{y_q}{\sqrt{2}} \bar{q}_{c_i} \frac{i \not{D}_{c_i \perp_i} - m_q}{n_{i+} \cdot D_{c_i}} \frac{\not{n}_{i+}}{2} q_{c_i} h_{c_i} + h.c. \right) \right]. \quad (3.35) \end{aligned}$$

The parameter renormalisation and decoupling constants, which are required in the following section, are listed in Appendix A.

3.2.1 Leading power amplitude

We integrate out the collinear scale with the virtuality of the order of m_t^2 and match the collinear fields onto the PDF-collinear fields [112–115] at leading power in the Λ_{QCD}^2/s

expansion, i.e. at leading twist. The relevant operator consists of two PDF-collinear gluon fields

$$\mathcal{J}_{\text{LP}}^{[i]}(t_1, t_2) = y_t^2 \mathcal{P}_{[i]}^{\mu\nu} \mathcal{A}_\mu^{\text{PDF}-c_1\perp_1}(t_1 n_{1+}) \mathcal{A}_\nu^{\text{PDF}-c_2\perp_2}(t_2 n_{2+}), \quad (3.36)$$

where the projectors $\mathcal{P}_{[i]}^{\mu\nu}$ are defined above in (3.9). We now work with $n_f = 5$ since the top quark is no longer an active degree of freedom below the scale m_t^2 and here y_t^2 is fixed at that scale. The matching at leading power reads

$$\langle H(q_3)H(q_4) | J_{\text{LP}}^{[i]}(0, 0, 0, 0) | g(q_1)g(q_2) \rangle = \mathcal{C} \langle 0 | \mathcal{J}_{\text{LP}}^{[i]}(0, 0) | g(q_1)g(q_2) \rangle, \quad (3.37)$$

where, as will be shown, the non-zero contribution to \mathcal{C} due to radiative corrections starts at the two-loop order, and consequently, for our loop induced process $gg \rightarrow HH$, it enters at the three-loop level. This term compensates precisely for the change in the cusp anomalous dimension when matching the theory with $n_f = 6$ on $n_f = 5$ at $\mu^2 \sim m_t^2$. The non-trivial structure of this term contradicts the claim in [86] that the matching is exact to all orders of perturbation theory. In fact, it is an interesting case of the IR matching (massification) procedure [76, 116–121]: at scales $\mu^2 \sim s$ the quarks are massless, but below m_t^2 the heavy top quarks can enter through soft loops, even though there are no external-state top quarks.

We obtain the form of \mathcal{C} at $\mathcal{O}(\alpha_s^2)$ starting from the bare matrix element of the operator for the theory on the left-hand side of our matching equation in (3.37) with one heavy and five light quarks provided in [117, 120]. The IR divergences of this matrix element correspond as usual to the UV renormalisation factors in the EFT below the scale m_t . We remove these divergences from the amplitudes on both sides of (3.37) and rearrange for the matching coefficient. In our conventions, the operator $J_{\text{LP}}^{[i]}$ is renormalised multiplicatively with $Z_{(n_f=6)}$ and the bare \mathcal{C} with $Z_{(n_f=5)}^{-1}$. We find that the renormalised \mathcal{C} is therefore given by

$$\begin{aligned} \mathcal{C} &= Z_{(n_f=5)}^{-1} Z_{(n_f=6)} \mathcal{Z}_g^{(m|0)}(m_t) \mathcal{S}(\{p\}, m_t) \\ &= 1 + \left(\frac{\alpha_s}{2\pi}\right)^2 \frac{C_A}{4} T_F \left(\frac{112}{27} \ln\left(-\frac{m_t^2}{s}\right) - \frac{28}{9} \zeta_3 - \frac{5}{27} \pi^2 + \frac{262}{27} \right) + \mathcal{O}(\alpha_s^3), \end{aligned} \quad (3.38)$$

where the anomalous dimensions required to construct renormalisation factors $Z_{(n_f=6)}$ and $Z_{(n_f=5)}$ are listed in Appendix A of [122] to sufficient accuracy. The cusp anomalous dimensions are known to four-loop order [123]. The $\mathcal{S}(\{p\}, m_t)$ term is taken from Eq. (2.3) of [120]. Similarly, $\mathcal{Z}_g^{(m|0)}(m_t)$ is constructed from terms in (2.6), (2.7), and (2.8), according to Eq. (2.2) of [120]. Moreover, to arrive at the result in (3.38), we have used the decoupling of the strong coupling constant given in (A.4) to write $\alpha_s^{(n_f=6)}$ appearing in the last three terms of (3.38) in terms of $\alpha_s^{(n_f=5)}$ for consistency with the strong coupling constant appearing in $Z_{(n_f=5)}^{-1}$. We note that this matching involves decoupling of the heavy top quark also from the α_s , which is explicitly present in operators given in (3.8) and (3.36).

We note that large logarithm $\ln(-m_t^2/s)$ appearing in (3.38) does not have its origin due to top-quark mass renormalisation but rather stems from the collinear anomaly. This tower of logarithms is universal and not specific to the $gg \rightarrow HH$ amplitude and can be obtained using rapidity renormalisation group techniques [124]. To perform the resummation of these logarithms, we note that our matching coefficient \mathcal{C} is, in fact, a composite object obeying rapidity type factorisation into jet and soft functions,

$$\mathcal{C} = J_{n_{1-}}(m_t^2; \mu^2, \nu^2/s) J_{n_{2-}}(m_t^2; \mu^2, \nu^2/s) S(m_t^2, \mu^2, \nu^2/m_t^2), \quad (3.39)$$

where the soft and jet functions are given by the matrix element of Wilson lines and collinear fields

$$\begin{aligned} S(m_t^2, \mu^2, \nu^2/m_t^2) &= \langle 0 | S^\dagger S | 0 \rangle \\ J_{n_{1-}}(m_t^2; \mu^2, \nu^2/s) &= \langle 0 | \mathcal{A}_{c_{1\perp 1}} | g_{c_1} \rangle \\ J_{n_{2-}}(m_t^2; \mu^2, \nu^2/s) &= \langle 0 | \mathcal{A}_{c_{2\perp 2}} | g_{c_2} \rangle, \end{aligned} \quad (3.40)$$

where S is the adjoint soft Wilson line $\mathcal{Y}_{i\mp}$ defined as

$$\mathcal{Y}_{i\mp}^{AB}(x) = \mathbf{P} \exp \left\{ g_s \int_{-\infty}^0 ds f^{ABC} n_{i-} A_s^C(x + sn_{\mp}) \right\}, \quad (3.41)$$

and the collinear building blocks are given in Eq. (3.4).

3.2.2 Next-to-leading power amplitude

Matching of subleading power operators at the scale $\mu^2 \sim m_t^2$ proceeds analogously to the analysis performed for the leading power operators in the section above. As before, the relevant operators below m_t^2 are constructed from PDF-collinear fields.

We recall that the next-to-leading power contributions are generated in each collinear sector, either through suppressed vector-type currents in the sectors collinear to the incoming gluons, or scalar type for the Higgses. To avoid repetition, we focus on the sector collinear to one of the initial state gluons, and the rest follows analogously. We first need the matrix element of the relevant subleading power operator with an external collinear gluon. Using the SCET Feynman rule for collinear gluon interaction with massive collinear quarks and a physical polarisation for the gluon, we find

$$\langle 0 | J_V^{\nu A}(r) | g^B(q_1) \rangle = -g_s \delta^{AB} m_t \frac{1}{4\epsilon} \Gamma[1 + \epsilon] e^{\epsilon\gamma_E} \left(\frac{\mu^2}{m_t^2} \right)^\epsilon \varepsilon_{\perp 1}^\nu(q_1), \quad (3.42)$$

where $J_V^{\nu A}(r)$ is the Fourier transform, see (3.23), of the vector-type subleading power operator given in (3.22) with momentum fraction r carried by the collinear quark in the NLP operator. Similarly, for the subleading power operator relevant in the Higgs sector, see (3.20), the matrix element calculation yields

$$\langle 0 | J_S(r) | H(q_3) \rangle = -\frac{y_t m_t \bar{r}}{2\sqrt{2}} \frac{1}{\epsilon} \Gamma[1 + \epsilon] e^{\epsilon\gamma_E} \left(\frac{\mu^2}{m_t^2} \right)^\epsilon. \quad (3.43)$$

Since at next-to-leading power the whole power suppression is generated in one of the collinear sectors, we now combine the NLP operator from above with leading power operators in the remaining three sectors. Analogously to (3.37), the complete NLP operator, which includes power suppression generated in each of the collinear sectors, has to be matched to leading-power (or leading twist) PDF-collinear operator. This can be obtained in a straightforward way using Eq. (3.40) for the leading power components of the operators and (3.42) as well as (3.43) for the power-suppressed sectors. We note that colour conservation and multipole-expansion of the soft-fields guarantees that the soft function appearing with NLP hard operator is identical to the one accompanying the leading power hard operator.

As remarked at the end of Section 3.1.1, there also exist contributions to the amplitude due to double insertions of $\mathcal{L}_{\xi q}$ Lagrangian terms through time-ordered products with lower-power currents [102]. An example where this type of contribution appears is the two-loop diagram considered in the MoR analysis in Section 2.1 where both of the loop momenta are soft. On the left-hand side of Fig. 13 we have drawn a corresponding EFT diagram to depict how this contribution is reproduced in SCET. Since each component of the soft momentum is scaling as λ , the interaction with a collinear mode results in a hard-collinear momentum scaling. Therefore, in the basis of operators we must also include leading power type operators with one hard-collinear field present in each direction. As noted above, with the regulator used in [81] these contributions start at one-loop order. Moreover, as the MoR analysis in the preceding section uncovered, at higher loop orders we see a cascade of modes in accordance with our expectations following the analysis of contributing modes with massive particles present [70]. Expressing the corresponding diagrams in the SCET set up, it becomes evident from the power counting that these contributions can only start to enter at NLP, and in fact, due to decoupling, we expect these contributions are further power suppressed. For example, the SCET representation of the three-loop graph with an ultra-collinear mode is shown on the right-hand side of Fig. 13. Using power counting for the objects entering the diagram, at first sight, it appears that this type of contribution can contribute at NLP. Indeed, diagram by diagram these diagrams can produce non-vanishing contributions at this order. However, focusing on the attachment of the soft-collinear gluon to the collinear loop, we notice a similarity with the case of leading power soft interaction coupling to a collinear loop, which has been studied in [113]. In that work, it has been shown that indeed the decoupling of soft and collinear effects in the leading power SCET Lagrangian is ultimately responsible for the explicit cancellation of such type of diagrams, since effectively, due to the decoupling, there is no external scale that can be associated with the collinear loop. For this reason, we expect that this type of contribution can only enter the power expansion of the Higgs pair production amplitude starting from NNLP. However, this can only be verified via an explicit calculation. In case there exists a mechanism which prevents the cancellation of such diagrams, it would be interesting to study in its own right. However, the lowest possible contribution is nonetheless an NLP effect and does not threaten our leading power analysis of the structure of the amplitude, which is the central focus of this work. This mechanism could have more

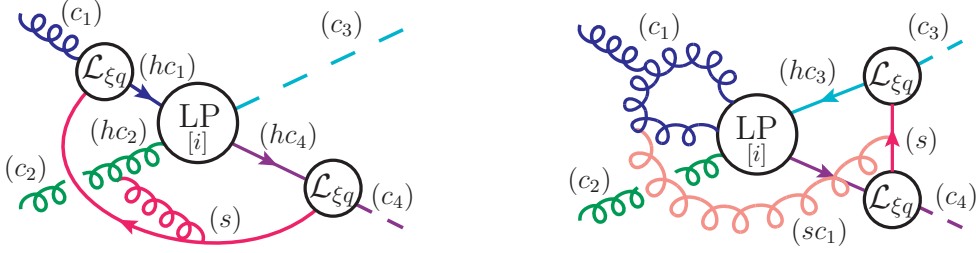


Figure 13: Effective field theory diagrams with scaling of internal lines indicated by labels (c_i) , (hc_i) , (s) , and (sc_i) corresponding to a collinear- q_i , hard-collinear- q_i , soft, and soft-collinear- q_i scaling, respectively. (left) Power suppressed contributions to the amplitude with time-ordered product insertions of subleading power Lagrangian terms and hard-collinear fields in the operator. This type of contribution reproduces the $(\ell_1, \ell_2) = (s, s)$ diagrams in Fig. 6. (right) Sample three-loop diagram (corresponding to one on the right-hand side of Fig. 7) power suppressed diagram with a new dynamical soft-collinear mode appearing at three-loop order, see cascading modes in [70]. In this process we expect that this contribution enters only at NNLP due to decoupling of leading power soft-collinear interactions.

interesting consequences in the case of $gg \rightarrow H$ amplitude studied in [86] since this process begins at NLP. Therefore, in case of non-cancellation of this type contributions from cascading modes appearing at higher orders, the process would receive corrections at the first order in the power counting. In general, for the derivation of the NLP factorisation formula for our process under consideration, all possible operators and structures need to be included. The explicit derivation of the NLP factorisation for $gg \rightarrow HH$ amplitude and resummation of the NLP corrections in m_t is left for future work.

3.3 Resummation

Having understood the structure of the amplitude, we are now ready to discuss the leading power resummation of the large logarithms of m_t contributing to the $gg \rightarrow HH$ amplitude in the high-energy limit. We discuss their numerical impact in Section 4. Resummation of the large logarithms is performed using renormalisation group equations (RGEs). At leading power, the RGE structure is remarkably simple due to the fact that the full leading power amplitude is equivalent to the hard-matching Wilson coefficient $C_{[i]}^{\text{LP}}(s, t, \mu)$. From the anomalous dimension of the leading power SCET operator given in (3.8) it follows that $C_{[i]}^{\text{LP}}(s, t, \mu)$ obeys the RGE

$$\frac{d}{d \ln \mu} C_{[i]}^{\text{LP}}(s, t, \mu) = \left(\Gamma_{\text{cusp}} \ln \frac{s}{\mu^2} + \gamma \right) C_{[i]}^{\text{LP}}(s, t, \mu). \quad (3.44)$$

The relevant anomalous dimensions are given by

$$\Gamma_{\text{cusp}} = \frac{\alpha_s}{2\pi} 2C_A + \mathcal{O}(\alpha_s^2), \quad \gamma = 0 + 2\gamma_m + \mathcal{O}(\alpha_s^2), \quad (3.45)$$

where α_s is the $\overline{\text{MS}}$ QCD coupling at the scale μ , the 0 in γ is the $\mathcal{O}(\alpha_s)$ contribution to the gluon collinear anomalous dimension, and $\gamma_m = \frac{3\alpha_s}{2\pi}C_F + \mathcal{O}(\alpha_s^2)$ is the anomalous dimension governing the running of the top-quark mass. Higher orders for γ_m can be found in [125]. The general solution to (3.44) reads

$$C_{[i]}^{\text{LP}}(s, t, \mu) = \exp \left[2S(\mu_h, \mu) - a_\gamma(\mu_h, \mu) \right] \left(\frac{s}{\mu_h^2} \right)^{-a_\Gamma(\mu_h, \mu)} C_{[i]}^{\text{LP}}(s, t, \mu_h), \quad (3.46)$$

where the auxiliary functions are given by [126]

$$S(\nu, \mu) = - \int_{\alpha_s(\nu)}^{\alpha_s(\mu)} d\alpha \frac{\Gamma_{\text{cusp}}(\alpha)}{\beta(\alpha)} \int_{\alpha_s(\nu)}^{\alpha} \frac{d\alpha'}{\beta(\alpha')}, \quad (3.47)$$

$$a_\Gamma(\nu, \mu) = - \int_{\alpha_s(\nu)}^{\alpha_s(\mu)} d\alpha \frac{\Gamma_{\text{cusp}}(\alpha)}{\beta(\alpha)}, \quad a_\gamma(\nu, \mu) = - \int_{\alpha_s(\nu)}^{\alpha_s(\mu)} d\alpha \frac{\gamma(\alpha)}{\beta(\alpha)}. \quad (3.48)$$

At this point it is worthwhile to discuss the fate of the different types of logarithmic corrections captured by our solution. Firstly, the function $S(\mu_h, \mu)$ contains logarithms of the type $\ln^2(\mu/\mu_h)$ with a C_A colour prefactor. This type of logarithms does not appear in the $\mathcal{O}(\alpha_s^2)$ amplitude results of [51] due to the fact that they are of IR origin and are cancelled in the process of removing IR poles using Catani's scheme [127]. This is a scheme choice for defining finite remainder of the amplitude. The SCET approach enables more natural implementation in the $\overline{\text{MS}}$ scheme which generalises easily to all orders. Indeed, as described above, we perform matching at the scale $\mu^2 \sim m_t^2$ to the relevant operator with PDF-collinear fields given in (3.36). Therefore, the structure of these logarithms is reflected in the running also below the scale $\mu^2 \sim m_t^2$ and ultimately these corrections reside in the long-distance scales appearing in the observables, and PDFs at the scale Λ_{QCD} . Concretely, we can again write down a formal solution of the RGE for the matching coefficient below m_t which follows from the anomalous dimension of the operator in (3.36), this time the natural reference scale is a low-energy scale $\mu_s \sim \Lambda_{\text{IR}}$

$$C_{[i]}^{\text{LP}}(s, t, \mu) = \exp \left[2S(\mu_s, \mu) - a_\gamma(\mu_s, \mu) \right] \left(\frac{\Lambda_{\text{IR}}^2}{\mu_s^2} \right)^{-a_\Gamma(\mu_s, \mu)} C_{[i]}^{\text{LP}}(s, t, \mu_s), \quad (3.49)$$

and the strong coupling constant present in these anomalous dimensions of the functions defined in (3.47) and (3.48) is evaluated in the five-flavour scheme. This solution can be used to run from the low scale to m_t where it must be matched to the high-energy theory. In the matching procedure we must also take care of the massification logarithms $\propto C_A \ln(-m_t^2/s)$ starting at $\mathcal{O}(\alpha_s^3)$ in the amplitude which arise due to soft massive top quarks appearing in loop corrections at this scale. These corrections are universal and have already been provided in Eq. (3.38). They can be resummed to all orders using

rapidity RGE. Last, and most pertinent to the problem at hand, are the logarithms originating in the top-quark mass renormalisation procedure arriving with a C_F colour prefactor. Since there are no other sources of logarithms involving the top-quark mass at leading power, as we have shown in this article, these are now be predicted to all orders in α_s using (3.46).

4 Controlling scheme uncertainties

In this section we discuss the impact of our MoR and EFT analysis on the uncertainty budget of double Higgs production via gluon-fusion. To summarise, the structure of the leading power amplitude is remarkably simple: as observed previously at NLO in [39], it turns out that the leading logarithms to all orders arise only from the renormalisation of the top-quark mass, which itself is well known in the literature. At next-to-leading logarithmic accuracy, there are additional contributions from universal IR matching (massification), which start contributing to the amplitude at NNLO. Our analysis provides a systematic understanding of the leading power leading logarithmic structure.

To quantify the numerical effect of the leading power leading mass logarithms, we study their impact on the one-loop amplitude and the finite remainder of the two-loop virtual amplitude. The finite remainder of the two-loop amplitude is obtained after UV renormalisation and IR subtraction. We begin by defining the two-loop remainder and briefly recapping how it is affected by changes in the top-quark mass scheme. As described in Section 2, we expand each of the bare form factors A_i as a perturbative series in the bare strong coupling $\alpha_{s,0}$,

$$A_i = \left(\frac{\alpha_{s,0}}{2\pi}\right) A_i^{(0)}(m_{t,0}^2) + \left(\frac{\alpha_{s,0}}{2\pi}\right)^2 A_i^{(1)}(m_{t,0}^2) + \mathcal{O}(\alpha_{s,0}^3), \quad (4.1)$$

where $m_{t,0}$ is the bare top-quark mass. The UV renormalisation is then performed by re-expressing the bare quantities in terms of their renormalised counterparts according to the formulae,

$$\alpha_{s,0} \equiv \alpha_s Z_{\alpha_s} S_\epsilon^{-1} \left(\frac{\mu_R^2}{\mu_0^2}\right)^\epsilon, \quad m_{t,0}^2 \equiv m_t^2 Z_m, \quad (4.2)$$

with $S_\epsilon = (4\pi)^\epsilon e^{-\gamma_E \epsilon}$, and multiplying the amplitude with $Z_G^{1/2}$ for each external gluon as dictated by the LSZ formula. The renormalisation constants can be expanded in α_s as, $Z_X = 1 + \left(\frac{\alpha_s}{2\pi}\right) \delta Z_X + \mathcal{O}(\alpha_s^2)$, with $X = \alpha_s, G, m$. Using the above prescription, the renormalised amplitude can then be written as,

$$\begin{aligned} A_i^{\text{ren}} = & S_\epsilon^{-1} \left(\frac{\mu_R^2}{\mu_0^2}\right)^\epsilon \left(\frac{\alpha_s}{2\pi}\right) A_i^{(0)}(m_t^2) \\ & + S_\epsilon^{-1} \left(\frac{\mu_R^2}{\mu_0^2}\right)^\epsilon \left(\frac{\alpha_s}{2\pi}\right)^2 \left[(\delta Z_G + \delta Z_{\alpha_s}) A_i^{(0)}(m_t^2) + \delta Z_m m_t^2 \frac{\partial A_i^{(0)}(m_t^2)}{\partial m_t^2} \right] \end{aligned}$$

$$+ S_\epsilon^{-2} \left(\frac{\mu_R^2}{\mu_0^2} \right)^{2\epsilon} \left(\frac{\alpha_s}{2\pi} \right)^2 A_i^{(1)}(m_t^2) + \mathcal{O}(\alpha_s^3). \quad (4.3)$$

where we have expanded in α_s and neglected terms of order α_s^3 . The mass counterterm amplitude is defined as,

$$A_i^{(0),\text{mct}}(m_t^2) \equiv m_t^2 \frac{\partial A_i^{(0)}(m_t^2)}{\partial m_t^2}. \quad (4.4)$$

It is often convenient to compute the derivative of the one-loop amplitude with respect to the top-quark mass using mass counterterm insertions.

Explicit expressions for the strong coupling and gluon wave-function renormalisation constants are given in Appendix A. The most relevant renormalisation constant for the present work is that of the top-quark mass. In the existing literature on Higgs pair production the top-quark mass has been renormalised in either the OS or $\overline{\text{MS}}$ renormalisation schemes, the corresponding renormalisation constants are given by [128, 129],

$$\delta Z_m^{\text{OS}} = C_F \left(-\frac{3}{\epsilon} - 4 \right) \left(\frac{\mu_R^2}{m_t^2} \right)^\epsilon, \quad \delta Z_m^{\overline{\text{MS}}} = C_F \left(-\frac{3}{\epsilon} \right) \left(\frac{\mu_R^2}{\mu_t^2} \right)^\epsilon, \quad (4.5)$$

with the colour factor $C_F = (N_c^2 - 1)/(2N_c)$.

Collecting the terms of Eq. (4.3) according to the order in α_s , we can write

$$A_i^{\text{ren}} = \left(\frac{\alpha_s}{2\pi} \right) A_i^{(0),\text{ren}}(m_t^2) + \left(\frac{\alpha_s}{2\pi} \right)^2 A_i^{(1),\text{ren}}(m_t^2) + \mathcal{O}(\alpha_s^3), \quad (4.6)$$

$$A_i^{(0),\text{ren}}(m_t^2) = S_\epsilon^{-1} \left(\frac{\mu_R^2}{\mu_0^2} \right)^\epsilon A_i^{(0)}(m_t^2), \quad (4.7)$$

$$A_i^{(1),\text{ren}}(m_t^2) = S_\epsilon^{-2} \left(\frac{\mu_R^2}{\mu_0^2} \right)^{2\epsilon} A_i^{(1)}(m_t^2) + S_\epsilon^{-1} \left(\frac{\mu_R^2}{\mu_0^2} \right)^\epsilon \left[(\delta Z_G + \delta Z_{\alpha_s}) A_i^{(0)}(m_t^2) + \delta Z_m A_i^{(0),\text{mct}}(m_t^2) \right], \quad (4.8)$$

The IR subtraction can be performed using the $I_1(\epsilon)$ operator of a given IR subtraction scheme (e.g. q_T , Catani, Catani-Seymour, SCET, ...). We write,

$$A_i^{\text{fin}}(m_t^2) = \left(\frac{\alpha_s}{2\pi} \right) A_i^{(0),\text{fin}}(m_t^2) + \left(\frac{\alpha_s}{2\pi} \right)^2 A_i^{(1),\text{fin}}(m_t^2) + \mathcal{O}(\alpha_s^3), \quad (4.9)$$

$$A_i^{(0),\text{fin}}(m_t^2) = A_i^{(0),\text{ren}}(m_t^2), \quad (4.10)$$

$$A_i^{(1),\text{fin}}(m_t^2) = A_i^{(1),\text{ren}}(m_t^2) - I_1(\epsilon) A_i^{(0),\text{ren}}(m_t^2). \quad (4.11)$$

Our “full” results are obtained using all available terms of the analytic high-energy/small-mass expansion of Ref. [51], which was computed using the Catani IR subtraction

scheme [127] after subtracting a scale dependent logarithm (see Eq. (13) and (14) of Ref. [51]). For an expansion in $\alpha_s/(2\pi)$, their IR subtraction operator can be written to finite order in ϵ as,

$$I_1^{\text{Catani}'}(\epsilon) = -\frac{C_A}{\epsilon^2} - \frac{1}{\epsilon} \left[\beta_0 + C_A \ln \left(\frac{\mu_R^2}{-s - i\delta} \right) \right] + C_A \left(\frac{\pi^2}{12} - \frac{1}{2} \ln^2 \left(\frac{\mu_R^2}{-s - i\delta} \right) \right) + \mathcal{O}(\epsilon). \quad (4.12)$$

with $\delta \rightarrow 0_+$ and $\beta_0 = 11C_A/6 - 2/3T_F n_f$. The conversion to the SCET subtraction scheme of Ref. [122] involves dropping the finite terms of Eq. (4.12), explicitly,

$$A_i^{(1),\text{SCET}} = A_i^{(1),\text{Catani}'} + \Delta I_{\text{SCET}} A_i^{(0),\text{ren}}, \quad (4.13)$$

$$\Delta I_{\text{SCET}} = I_1^{\text{Catani}'} - I_1^{\text{SCET}} = C_A \left(\frac{\pi^2}{12} - \frac{1}{2} \ln^2 \left(\frac{\mu_R^2}{-s - i\delta} \right) \right) + \mathcal{O}(\epsilon), \quad (4.14)$$

where $A_i^{(1),\text{Catani}'}$ is the finite amplitude with $I_1(\epsilon)$ given by (4.12), and $A_i^{(1),\text{SCET}}$ is the finite amplitude obtained with $I_1(\epsilon)$ that contains only the pole parts of (4.12). For the results presented here, we use the SCET scheme with $\mu_R^2 = s$. We also set the top-quark mass renormalisation scale $\mu_t^2 = s$.

We now turn our attention to the all-order structure of the small top-quark mass power-expanded y_t^2 box contribution to the $pp \rightarrow HH$ amplitude, which in the $\overline{\text{MS}}$ scheme can be written as follows,

$$\text{LO} : \quad \alpha_s y_t^2 (\mathbf{c}_0 + m_t n_0), \quad (4.15)$$

$$\text{NLO} : \quad \alpha_s^2 y_t^2 (\mathbf{a}_1 l_\mu + \mathbf{c}_1 + m_t n_1), \quad (4.16)$$

$$\text{NNLO} : \quad \alpha_s^3 y_t^2 (\mathbf{a}_2 l_\mu^2 + \mathbf{b}_2 l_m + \mathbf{c}_2 + m_t n_2), \quad (4.17)$$

$$\text{N}^3\text{LO} : \quad \alpha_s^4 y_t^2 (\mathbf{a}_3 l_\mu^3 + \mathbf{b}_3 l_m^2 + \mathbf{d}_3 l_m + \mathbf{c}_3 + m_t n_3), \quad (4.18)$$

$$\text{N}^i\text{LO} : \quad \alpha_s^{i-1} y_t^2 (\mathbf{a}_i l_\mu^i + \mathbf{b}_i l_m^{i-1} + \mathbf{d}_i l_m^{i-2} + \dots + \mathbf{c}_i + m_t n_i). \quad (4.19)$$

with $l_\mu = \ln(\mu_t^2/s)$ and l_m contains both $\ln(\mu_t^2/s)$ and $\ln(m_t^2/s)$ logarithms. In our expressions, we have suppressed the dependence on the Higgs boson mass and consider only the leading (hard) term in the expansion around small Higgs boson mass. The green terms, $\mathbf{a}_i l_\mu^i$, are the small-mass leading power leading logarithms, they are known from the renormalisation group running of the top-quark mass. The orange terms, $\mathbf{b}_i l_m^{i-1}$, are the leading power next-to-leading logarithms, they receive a contribution from the running of the top-quark mass and from massification. The leading power constant coefficients \mathbf{c}_0 and \mathbf{c}_1 , highlighted in blue, are known from the one- and two-loop fixed order calculation in the small mass limit. The three-loop leading power constant coefficient, \mathbf{c}_2 , is currently unknown, but it can be obtained from a purely massless three-loop computation since the leading power amplitude receives contributions only from the hard region (i.e. a simple Taylor expansion around $m_t = 0$), the relevant master integrals are

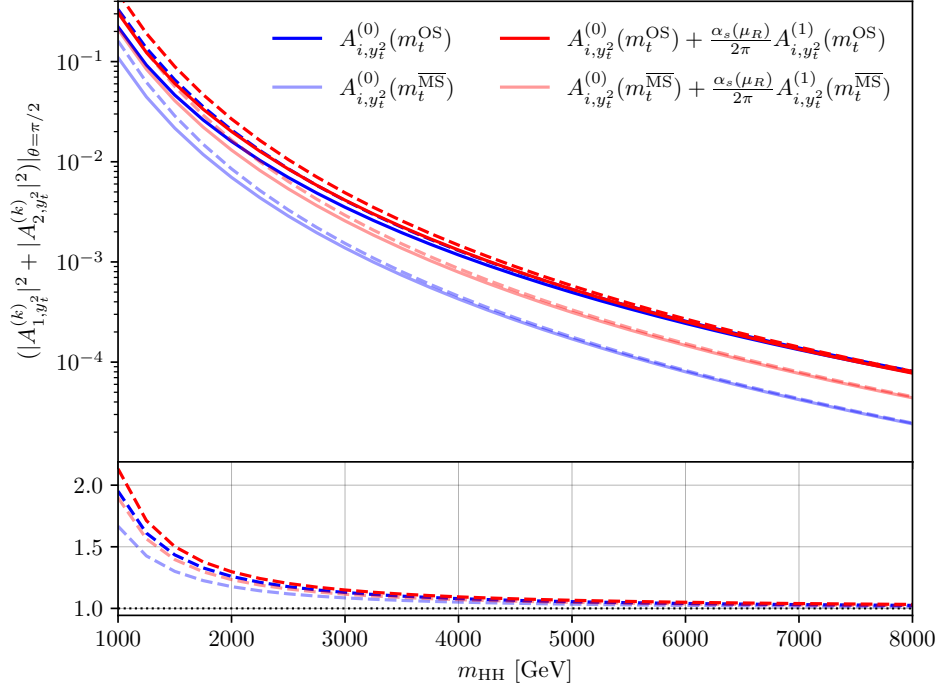


Figure 14: Plot demonstrating the validity of leading power expansion. Solid lines represent the full contribution to the LO and NLO squared amplitudes. The dark- and light-blue lines contain leading order one-loop amplitudes with top-quark mass in the OS and $\overline{\text{MS}}$ scheme, respectively. The dark- and light-red lines show the same at two-loop order. The dashed lines contain the corresponding contributions at leading power in m_t^2/s . In the bottom panel we plot the ratio of the leading power to the corresponding unexpanded line. It is apparent that at high-energies the leading power version of each of the lines captures the behaviour of the corresponding full contribution.

known [130, 131]. The four-loop next-to-next-to-leading power logarithm coefficient, \mathbf{d}_3 , is currently unknown but can be obtained from knowledge of the three-loop constant \mathbf{c}_2 , once it has been computed. The terms n_0 and n_1 contain the one-loop and two-loop beyond leading power (i.e. next-to-leading power, next-to-next-to-leading power, ...) results, the n_0 term can be obtained at any power by expanding the analytic one-loop result, the first 118 terms in the m_t expansion of n_1 are known [51, 53]. The next-to-leading power and beyond coefficients starting from three-loops (i.e. n_3, n_4, \dots) are currently unknown, understanding their structure would require the extension of the SCET factorisation theorem to NLP for $2 \rightarrow 2$ scattering of gluon and Higgs particles along the lines of the considerations presented in Section 3.

As a first step in our phenomenological analysis, we test the validity of the leading power expansion of the amplitudes at high-energies. In Fig. 14, we demonstrate that in the very high-energy regime the leading power ($y_t^2 m_t^0$) amplitude provides a good approximation of the full result. In this figure, we plot the sum of the squared amplitude

for different cases. Namely, contributions to A_{1,y_t^2} and A_{2,y_t^2} at one- and two-loops, both for the top-quark mass in the OS and $\overline{\text{MS}}$ schemes. For the conversion of the top-quark mass from the OS to the $\overline{\text{MS}}$ scheme and the running of α_s , we use the codes `RunDec` and `CRunDec` [132, 133]. Note that when squaring the two-loop amplitude, we actually compute the interference between the one- and two-loop amplitudes, $2 \text{Re}[A_{i,y_t^2}^{(0)}(A_{i,y_t^2}^{(1)})^*]$. Solid lines are obtained using the expansion up to $\mathcal{O}(m_t^{16})$, including finite m_H effects up to $\mathcal{O}(m_H^2)$, as provided in Ref. [51]. This expansion is known to reproduce the full NLO result with very high accuracy for the $\sqrt{s} \gtrsim 1$ TeV region considered here. The dashed lines contain the corresponding terms expanded to leading power in m_t^2/s . We see that at high-energies the leading power terms are responsible for the behaviour of the full amplitudes, i.e. the subleading power terms are negligible above the energy scale of around 4 TeV. At the lower end of the energy spectrum the leading power approximation breaks down and the subleading power terms become more important, as expected. We also note that the results plotted for the amplitudes at same order, but with top-quark mass in different schemes, give rise to lines which do not overlap. The difference between these lines is taken as the top-quark mass scheme uncertainty, as advocated in Ref. [40]. In Appendix C, we additionally display the comparison between the full and leading power results for the real and imaginary of each form factor. We remark that the uncertainty presented in [40] is for the NLO $pp \rightarrow HH$ cross section, includes the virtual and real corrections. In our analysis we consider solely the virtual corrections.

We plot the uncertainty bands due to the choice of the top-quark mass scheme at one- and two-loops in Fig. 15a. We see that at leading order the uncertainty on the virtual amplitude is 60–70% (blue band) across the spectrum at high-energies, where the small- m_t^2 expansion is valid. With inclusion of the higher order corrections the uncertainty is reduced to around 40% (red band).

At this point we consider again the structure of the amplitude at higher orders which, is laid out between Eqs. (4.15) and (4.19). In the $\overline{\text{MS}}$ scheme, the logarithms $\mathbf{a}_i \mathbf{l}_\mu^i$ depend on the scale μ_t which can be set to the order of s , rendering these explicit logarithms small. The dependence on the large ratio of scales, m_t^2/s , is captured to all orders in α_s implicitly through the running of top-quark mass. Since the bare top-quark mass can be renormalised in either scheme as in (4.2), the conversion factor between OS and $\overline{\text{MS}}$ schemes is defined through the ratio of the corresponding Z -factors

$$\frac{m(\mu)}{M} = \frac{Z_m^{\text{OS}}}{Z_m^{\overline{\text{MS}}}} \equiv z_m(\mu). \quad (4.20)$$

The quantity $z_m(\mu)$ has the following perturbative expansion

$$z_m(\mu) = \sum_{n \geq 0} \left(\frac{\alpha_s(\mu)}{2\pi} \right)^n (z_m^n(M) + z_m^{n,\log}(\mu)). \quad (4.21)$$

In the above equation, $z_m^{n,\log}(\mu)$ contains only the μ -dependent terms which vanish for $\mu = M$. The constant parts, $z_m^n(M)$, have been computed up to four-loop order in

Ref. [134], in our conventions they have an additional factor of 2 per loop order. Since the $gg \rightarrow HH$ amplitude is known at NLO, the conversion is typically truncated at the first order, as done in the plot in Fig. 14, where we make use of,

$$z_m(\mu) = 1 + \frac{\alpha_s(\mu)}{2\pi} \left(-2C_F - \frac{3}{2}C_F \ln \frac{\mu^2}{M^2} \right) + \mathcal{O}(\alpha_s^2), \quad (4.22)$$

which leads to a wide discrepancy between the two schemes. Importantly, we can now also identify precisely why this is the case. Namely, the large logarithms which are captured implicitly for the $\overline{\text{MS}}$ scheme, have only partially been restored in the corresponding OS result through the truncated conversion factor. Indeed, only the first leading power leading logarithm is captured correctly using Eq. (4.22). We argue that the discrepancy between the two schemes obtained in this manner should not form part of the uncertainty budget for the amplitude, since the leading logarithms (and beyond) in the conversion factor are in fact *known* to all orders in perturbation theory and can be reinstated using the renormalisation group equations for $m(\mu)$ and $\alpha_s(\mu)$. In the previous sections we have found that this is the only source of leading power leading logarithms, such that we can supplement the OS result with a complete and consistent tower of these logarithms. In order to do this, we first resum the leading logarithms appearing in Eq. (4.22) to all orders, this gives the scheme conversion formula,

$$m^{\text{LL}}(\mu) = M \exp \left[a_{\gamma_m}^{\text{LL}}(\mu) \right] z_m(M), \quad a_{\gamma_m}^{\text{LL}}(\mu) = \frac{3C_F}{2\beta_0} \ln \left(1 - \frac{\alpha_s(\mu)}{2\pi} \beta_0 \ln \left(\frac{\mu^2}{M^2} \right) \right). \quad (4.23)$$

As a check, expanding the exponential in powers of α_s gives the logarithms quoted in Appendix C of [134] up to the fourth loop order. Once these logarithms are included to all orders, either explicitly in the amplitude or implicitly in the definition of the running quark mass, the remaining mass scheme uncertainty is due only to subleading logarithms at leading power and subleading power terms. In our numerical results, in addition to the leading logarithms generated by $a_{\gamma_m}^{\text{LL}}$, we take only the leading constant term in z_m , i.e. z_m^0 .

We now define resummed amplitudes in the OS scheme supplemented by the complete tower of leading power leading mass logarithms, they are given by,

$$A_{i,y_t^2}^{(j,\text{LL})}(m_t^{\text{OS}}) = \left(\frac{m^{\text{LL}}(\mu_t)}{m_t^{\text{OS}}} \right)^2 A_{i,y_t^2}^{(j)}(m_t^{\text{OS}}). \quad (4.24)$$

Note that since the power expansion of the amplitudes starts at order $y_t^2 m_t^0 \sim m_t^2$ the ratio $(m^{\text{LL}}(\mu_t)/m_t^{\text{OS}})^2$ effectively restores the (green) tower of leading logarithms in Eqs. (4.15)–(4.19), leaving all other contributions in the original OS scheme.

We plot the comparison of the $A_{i,y_t^2}^{(j,\text{LL})}(m_t^{\text{OS}})$ amplitudes to those in the $\overline{\text{MS}}$ scheme in Fig. 15b. We observe a very significant reduction in the size of the uncertainty bands. The behaviour is expected, since as we argued the discrepancy between the results for the amplitudes obtained in different schemes is due to large logarithms taken into account

s [GeV]	LO		NLO	
	OS [fb]	OS ^{LL} [fb]	OS [fb]	OS ^{LL} [fb]
3000.0	$(3.52 \times 10^{-3})^{+0\%}_{-60.8\%}$	$(1.80 \times 10^{-3})^{+0\%}_{-23.6\%}$	$(4.14 \times 10^{-3})^{+0\%}_{-37.9\%}$	$(2.68 \times 10^{-3})^{+0\%}_{-4.2\%}$
4000.0	$(1.17 \times 10^{-3})^{+0\%}_{-63.7\%}$	$(5.70 \times 10^{-4})^{+0\%}_{-25.1\%}$	$(1.32 \times 10^{-3})^{+0\%}_{-39.9\%}$	$(8.23 \times 10^{-4})^{+0\%}_{-3.9\%}$
5000.0	$(4.96 \times 10^{-4})^{+0\%}_{-65.7\%}$	$(2.30 \times 10^{-4})^{+0\%}_{-26.0\%}$	$(5.34 \times 10^{-4})^{+0\%}_{-41.2\%}$	$(3.25 \times 10^{-4})^{+0\%}_{-3.5\%}$
6000.0	$(2.44 \times 10^{-4})^{+0\%}_{-67.1\%}$	$(1.09 \times 10^{-4})^{+0\%}_{-26.7\%}$	$(2.54 \times 10^{-4})^{+0\%}_{-42.1\%}$	$(1.52 \times 10^{-4})^{+0\%}_{-3.2\%}$
7000.0	$(1.33 \times 10^{-4})^{+0\%}_{-68.3\%}$	$(5.80 \times 10^{-5})^{+0\%}_{-27.2\%}$	$(1.35 \times 10^{-4})^{+0\%}_{-42.8\%}$	$(7.92 \times 10^{-5})^{+0\%}_{-2.8\%}$
8000.0	$(7.86 \times 10^{-5})^{+0\%}_{-69.2\%}$	$(3.34 \times 10^{-5})^{+0\%}_{-27.6\%}$	$(7.76 \times 10^{-5})^{+0\%}_{-43.3\%}$	$(4.51 \times 10^{-5})^{+0\%}_{-2.4\%}$

Table 3: Comparison of the OS and OS^{LL} scheme (see text) results and the remaining mass scheme uncertainty for the squared/interfered virtual amplitudes at one- and two-loop order as a function of s at fixed $\theta = \frac{\pi}{2}$. Note that these numbers do not include the real radiation and subtraction term contributions.

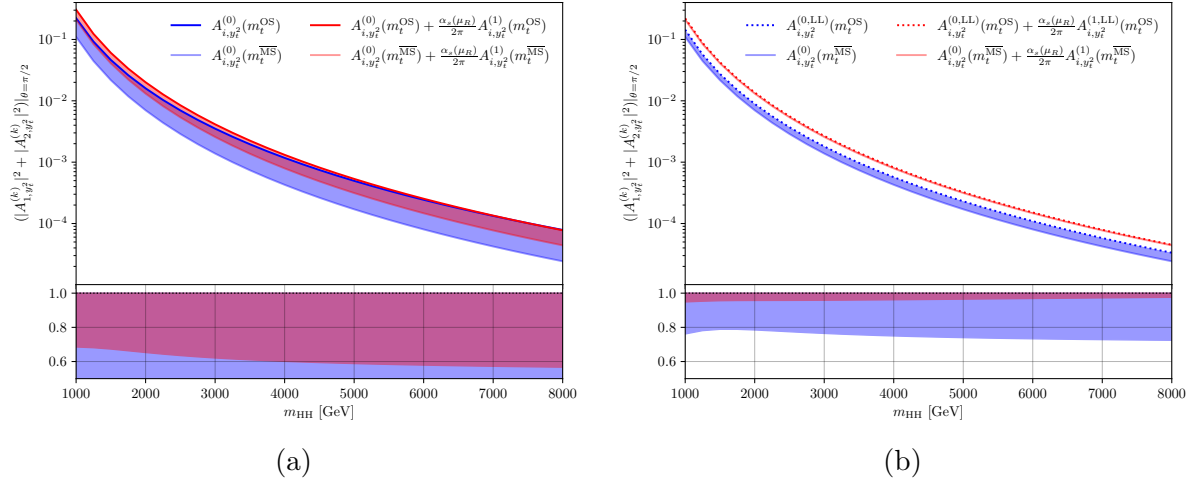


Figure 15: Comparison of results for the sum of the squared form factors at one- and two-loop order where the top-quark mass is renormalised in the $\overline{\text{MS}}$ and OS (panel (a)) and the same quantities with the OS result supplemented by the resummed tower of leading power leading logarithms (panel (b)). Significant reduction in the size of the uncertainty due to the choice of the top-quark mass renormalisation scheme is observed.

implicitly in the $\overline{\text{MS}}$ scheme but not in OS, which we have now explicitly reinstated via Eq. (4.24). The size of the mass scheme uncertainty, defined as the difference between the OS or OS^{LL} result and the $\overline{\text{MS}}$ result, is given for several different energies in Table 3.

The uncertainty in the double Higgs production amplitudes due to the choice of the top-quark mass scheme can be further reduced through inclusion of terms constituting higher logarithmic running of the top-quark mass in the conversion factor, i.e. the $z(\mu)$ factor in Eq. (4.21). This improvement amounts to extension of Eq. (4.23) to subleading logarithmic accuracy. However, in order to formally keep control over next-to-leading logarithms we are also required to perform resummation of the logarithms arising due

to universal IR matching (massification) as discussed in Section 3.2. This series starts at the three-loop order and we provide the first logarithm in Eq. (3.38).

The predictions can also be improved through resummation of large top-quark mass logarithms at subleading powers, where their origin is more involved than at leading power as explored in our MoR analysis. Control over subleading power terms would supplement the predictions at lower values of the invariant mass of the double Higgs system where the leading power approximation is seen to break down in Fig. 14. We leave both the resummation of universal IR matching logarithms and subleading power terms for future studies.

5 Summary and outlook

One of the key objectives for the HL-LHC is to perform a measurement of the trilinear Higgs self-coupling [135]. Precise theoretical predictions for the relevant cross sections are of critical importance in this endeavour. However, as has been noted in the literature, theoretical predictions are currently dominated by the large uncertainty present due to the dependence of the corresponding amplitudes on the choice of the top-quark mass scheme and scale [40]. This uncertainty can be reduced by higher order perturbative calculations. However, retaining the full mass dependence in higher order calculations is extremely challenging. Curiously, it has also been observed that in the case of double Higgs production in gluon-gluon scattering, at high-energies, the logarithmic dependence of the leading power contribution at NLO is fully determined by the choice of the top-quark mass renormalisation scheme [40]. In the language of the MoR, this corresponds to the fact that only the hard region contributes to the leading power amplitude at this order.

In this work, we have systematically studied the contribution of different regions to the amplitudes. Utilising an automated tool, we found that at the level of *scalar integrals*, it is possible that many regions give rise to leading, and in certain cases, power-enhanced contributions. We also observed that at higher orders new modes appear, as is expected for amplitudes with massive internal lines [70]. However, it remains true that at the level of the *amplitude* the hard region captures the leading power behaviour of the $gg \rightarrow HH$ process. This behaviour can be understood to all orders in perturbation theory once we cast the problem in the effective field theory language and consider how power suppressed contributions arise. We use the SCET framework to build operators that capture the structure of the amplitude and find that regions other than the hard region can indeed give contributions to the amplitude, but, these can only arise at subleading powers due to helicity suppression. We explicitly demonstrate that there is no mixing of external gluons (or Higgs bosons) with leading power structures other than the hard region, and since helicity is conserved in the massless limit, this holds to all orders in perturbation theory. While we leave the derivation of an explicit factorisation formula at subleading power for future work, the upshot of our analysis is a proof that the logarithmic behaviour of the leading power amplitude can be predicted from the hard region and universal

contributions, i.e. the choice of renormalisation scheme for the top-quark mass and IR matching (massification).

Leveraging our newfound understanding of the origin of the large logarithms appearing in the leading power amplitudes, we analyse the implications for the top-quark mass scheme choice uncertainty. First, we see that indeed the leading power approximation captures the behaviour of the full amplitude well at sufficiently high-energies in both the OS and $\overline{\text{MS}}$ renormalisation schemes. Ref. [40] advocates that the mass scheme uncertainty for the amplitude can be estimated by taking the envelope of the results obtained in the OS and $\overline{\text{MS}}$ schemes. However, since the complete tower of leading mass logarithms is known at leading power, we argue that these logarithms should always be accounted for in the theoretical prediction and should *not* form part of the uncertainty budget. Following this reasoning, we include the complete set of leading logarithms into the OS result and find that for the squared/interfered virtual amplitude, the top-mass scheme uncertainty can be reduced from 65% to 25% at LO and from 40% to 4% at NLO.

Our handle on the mass scheme uncertainties can be further improved by including higher logarithmic evolution of the top-quark mass in the scheme conversion. Namely, retaining more of the known logarithms in the conversion factor between the OS and $\overline{\text{MS}}$ schemes which originate in the running of the top-quark mass. Moreover, the logarithms due to universal IR matching need to be resummed and included in the predictions before formal NLL accuracy for the result can be claimed at leading power. In our phenomenological study we also observe that the leading power approximation starts to break down at lower values for the invariant mass of the system where power corrections become important. Subleading power contributions have a much richer factorisation structure as we have uncovered in our MoR analysis and it will be interesting from the theoretical development point of view to extend the framework to next-to-leading power. To reduce the mass scheme uncertainty at and below the top-quark threshold, it may also prove useful to consider the all-order structure of mass corrections in a different expansion, for example, the heavy-top limit, the threshold expansion at $s \sim 4m_t^2$, or the small- p_T expansion.

Studies of the small mass expansion can be performed for related processes such as Higgs production in association with a Z boson, and Z boson pair production. In these cases, the structure of the mass dependent logarithms is more complicated already at leading power, which hints at a richer factorisation structure in the Therefore, a more involved EFT description and resummation is already needed at leading power. Nonetheless, the results for these processes are important from the phenomenological perspective of the HL-LHC theory precision targets.

Acknowledgements

We want to thank M. Schnubel for providing clarification on [86], and R.S. would like to thank C. Savoini for very helpful discussions about massification. S.E.J. and R.S. thank the ‘‘Quantum Field Theory at the Frontiers of the Strong Interaction’’ ESI workshop

in Vienna and the ‘‘EFT and multi-loop methods for advancing precision in collider and gravitational wave physics’’ workshop at the Munich Institute for Astro-, Particle and BioPhysics (MIAPbP), which is funded by the Deutsche Forschungsgemeinschaft (DFG, German Research Foundation) under Germany’s Excellence Strategy - EXC-2094 - 390783311, where parts of this work were completed. S.P.J. and S.E.J. were supported in part by STFC under grant ST/X003167/1 and the Royal Society University Research Fellowship (URF/R1/201268). R.S. is supported by the United States Department of Energy under Grant Contract DE-SC0012704. Figures were drawn with Jaxodraw [136].

A Renormalisation and decoupling constants

In this appendix, we reproduce parameter renormalisation and decoupling constants as required in the main text. The $\overline{\text{MS}}$ renormalisation constant for the strong coupling up to the two-loop order is given by

$$Z_{\alpha_s} = 1 - \left(\frac{\alpha_s^{(n_f)}}{2\pi} \right) \frac{\beta_0}{\epsilon} + \left(\frac{\alpha_s^{(n_f)}}{2\pi} \right)^2 \left(\frac{\beta_0^2}{\epsilon^2} - \frac{\beta_1}{4\epsilon} \right), \quad (\text{A.1})$$

where

$$\beta_0 = \frac{11}{6}C_A - \frac{4}{6}T_F n_f, \quad \beta_1 = \frac{17}{3}C_A^2 - \frac{10}{3}C_A T_F n_f - 2C_F T_F n_f. \quad (\text{A.2})$$

The on-shell gluon wave-function renormalisation is given by,

$$Z_g = 1 + \frac{\alpha_s^{(n_f)}}{2\pi} T_F n_h \left(-\frac{2}{3\epsilon} - \frac{2}{3} \ln \left(\frac{\mu^2}{m_t^2} \right) - \frac{1}{3} \epsilon \ln^2 \left(\frac{\mu^2}{m_t^2} \right) - \frac{\pi^2 \epsilon}{18} + \mathcal{O}(\epsilon^2) \right) + \mathcal{O}(\alpha_s^2), \quad (\text{A.3})$$

where n_f is the number of light quarks and n_h is the number of heavy quarks.

We also need the decoupling of the strong coupling constant, up to the first loop order it is given by [137],

$$\begin{aligned} \zeta_{\alpha_s} = 1 + \frac{\alpha_s}{2\pi} T_F \left(\frac{2}{3} \ln \left(\frac{\mu^2}{m_t^2} \right) + \frac{1}{3} \epsilon \ln^2 \left(\frac{\mu^2}{m_t^2} \right) + \frac{\pi^2}{18} \epsilon + \frac{1}{9} \epsilon^2 \ln^3 \left(\frac{\mu^2}{m_t^2} \right) \right. \\ \left. + \frac{\pi^2}{18} \epsilon^2 \ln \left(\frac{\mu^2}{m_t^2} \right) - \frac{2\zeta_3}{9} \epsilon^2 \right) + \mathcal{O}(\alpha_s^2). \end{aligned} \quad (\text{A.4})$$

for the case where we have only one heavy quark, the two-loop correction can be found in Eq. (A.4) of [138]. Additionally, we provide the collinear spinor expansion needed in matching calculations performed in Section 3.1.2

$$u(q) = \left(1 + \frac{\left(\not{q}_{\perp 1} + m_t \right) \not{n}_{1+}}{n_{1+} q} \frac{1}{2} \right) u_{c_1}(q),$$

$$v(q) = \left(1 + \frac{(\not{q}_{\perp 1} - m_t) \not{q}_{1+}}{n_{1+} q} \right) v_{c_1}(q). \quad (\text{A.5})$$

B Region expansion at two-loops

In this appendix, we provide the regions for the remaining two top-level topologies at two-loops drawn in Fig. 4. The regions for **P2** are given in Fig. 16 and regions for **NP2** are given in Fig. 17. The purely hard regions are omitted.

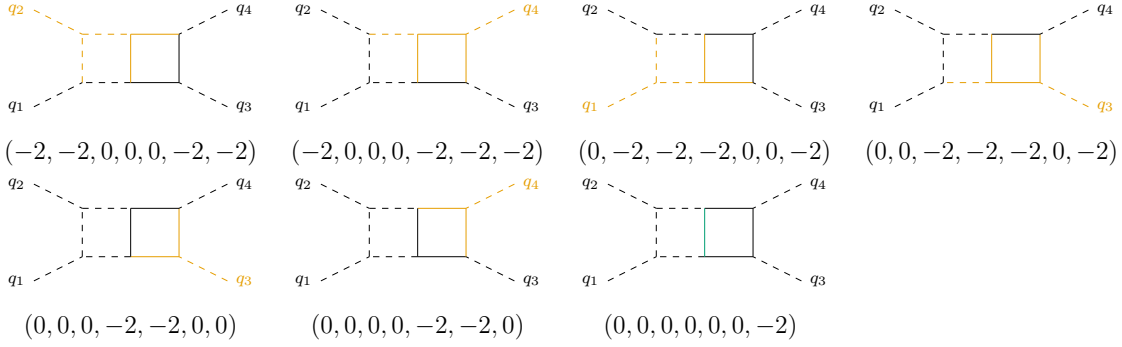


Figure 16: Regions for the two-loop diagram **P2** in Fig. 4. Propagators and external lines are coloured **orange** for the first collinear mode, **blue** for the second collinear mode, **green** for the soft modes, and **black** for the hard modes. Purely hard region is not depicted.

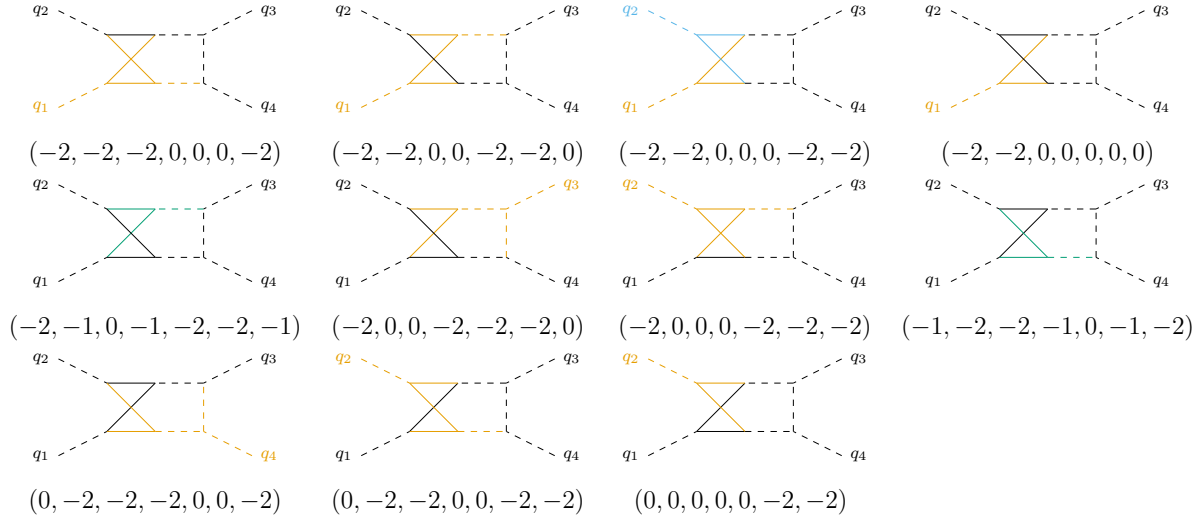


Figure 17: Regions for the two-loop diagram **NP2** in Fig. 4. Propagators and external lines are coloured **orange** for the first collinear mode, **blue** for the second collinear mode, **green** for the soft modes, and **black** for the hard modes. Purely hard region is not depicted.

C Amplitudes: Full vs Leading Power

Here, we present a breakdown of the contributions of each individual form factor, A_{1,y_t^2} and A_{2,y_t^2} , to the total amplitude. In Fig. 18, we plot the full contributions to the real and imaginary parts of A_{1,y_t^2} and A_{2,y_t^2} , and their leading power counterparts. For the case of the real parts, we see that the leading power terms for A_{1,y_t^2} exhibit a better agreement over wide range of the invariant mass of the system, m_{HH} , than the A_{2,y_t^2} amplitudes. For the real parts of A_{2,y_t^2} , including higher order effects extends the range of validity of the leading power approximation down approximately 2.5TeV, here the power suppressed effects will have a larger impact than in the case of A_{1,y_t^2} . In Fig. 19, we show the individual contributions from A_{1,y_t^2} and A_{2,y_t^2} at the amplitude-squared level, both show good agreement between full and leading power contributions.

In Fig. 20, we present the reduction in uncertainty due to the choice of the top-quark mass scheme, as described in the main text, for the individual form factors. This plot presents the breakdown of Fig. 15 into the separate form factors, A_{1,y_t^2} and A_{2,y_t^2} .

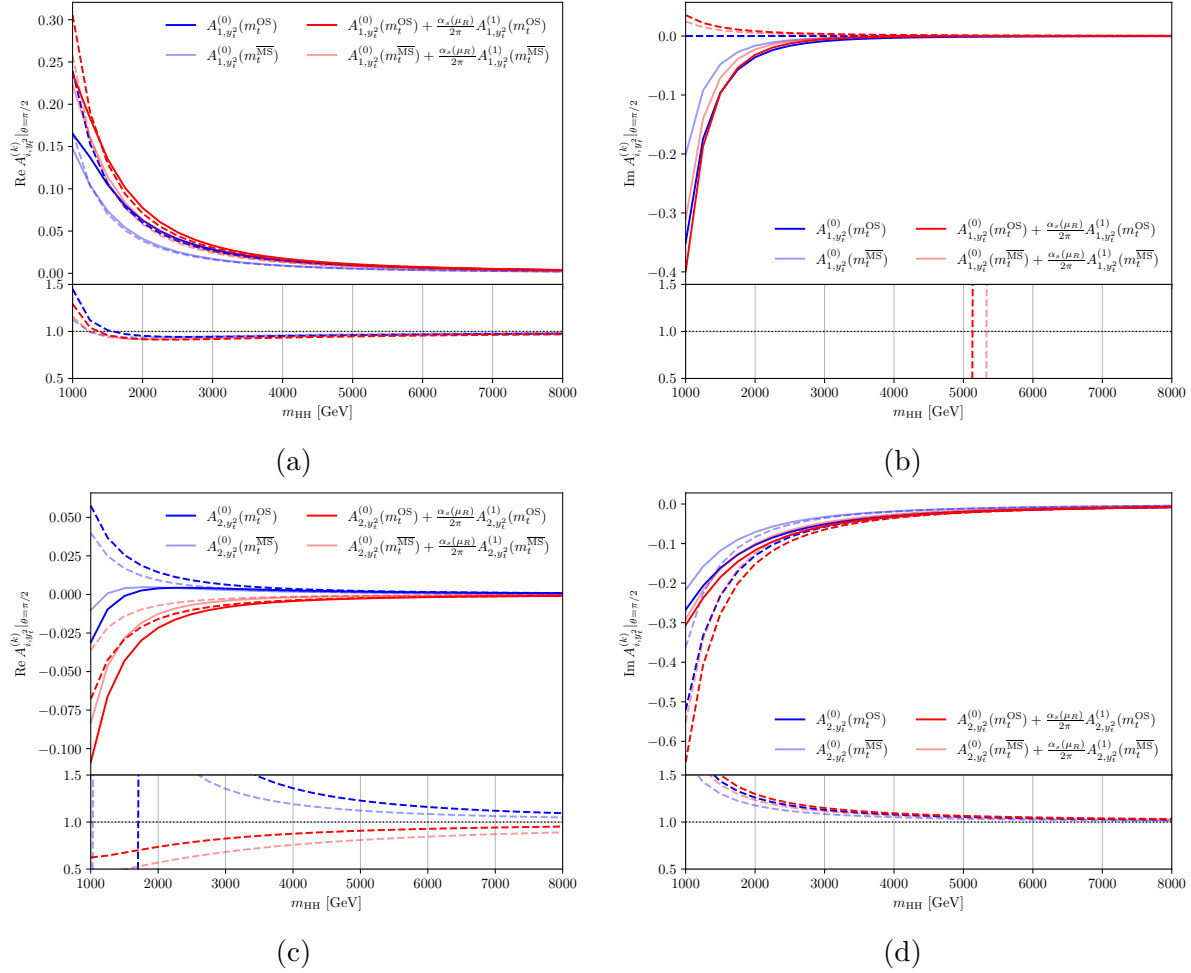


Figure 18: Plots analogous to Fig. 14, testing the validity of the leading power expansion at one- and two-loop. Solid lines represent the full contributions and dotted lines are only the leading power terms. Here we show a breakdown of the different parts: In panels (a) and (b) we have the real and imaginary contributions to A_{1,y_t^2} , respectively. In panels (c) and (d) we show the same information for the A_{2,y_t^2} form factor.

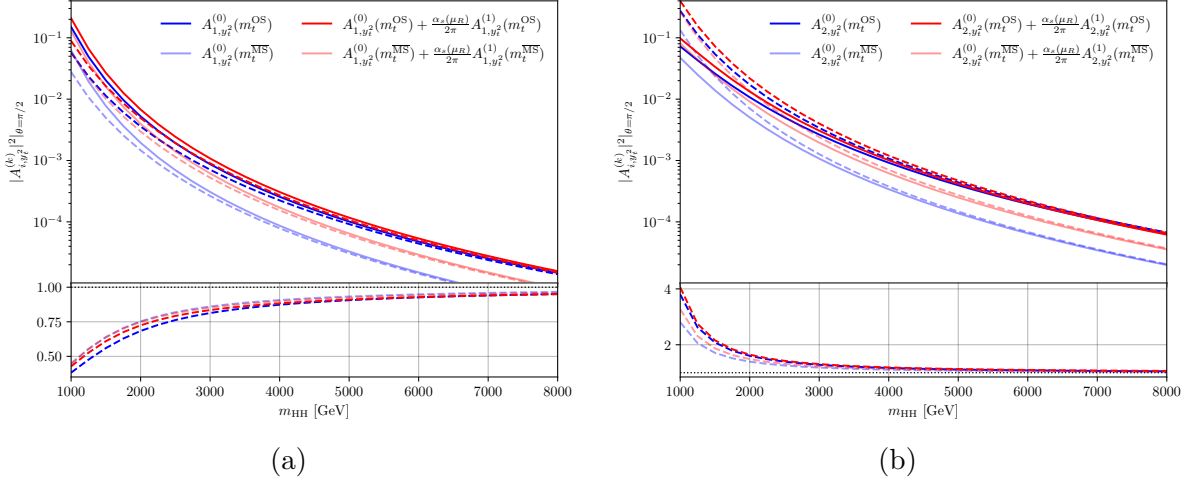


Figure 19: Comparison of full versus the leading-power result at one- and two-loop for square of each form factor. Solid lines represent the full result and dotted lines the leading power contributions.

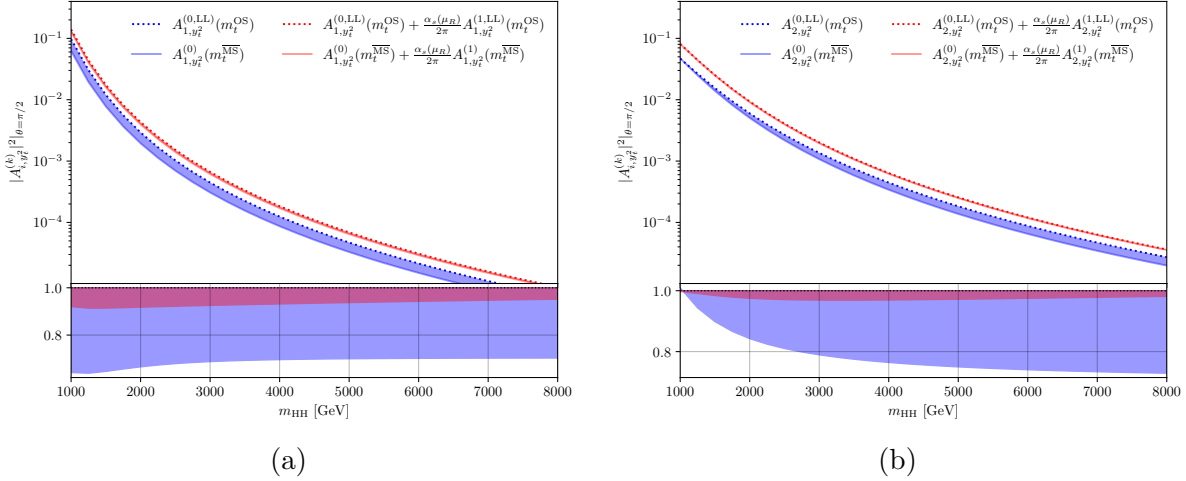


Figure 20: Plots showing the uncertainty bands due to the choice of the top-quark mass renormalisation scheme after supplementing the OS result with leading large logarithms according to the prescription described in the main text. Plot is analogous to Fig. 15b, but instead of the sum of the square of the form factors, here we show the A_{1,y_t^2} and A_{2,y_t^2} squared form factors individually in panels (a) and (b), respectively.

References

- [1] S. Badger, H. B. Hartanto and S. Zoia, *Two-Loop QCD Corrections to $Wb\bar{b}$ Production at Hadron Colliders*, *Phys. Rev. Lett.* **127** (2021) 012001, [[2102.02516](#)].
- [2] S. Abreu, F. Febres Cordero, H. Ita, M. Klinkert, B. Page and V. Sotnikov, *Leading-color two-loop amplitudes for four partons and a W boson in QCD*, *JHEP* **04** (2022) 042, [[2110.07541](#)].
- [3] H. B. Hartanto, R. Poncelet, A. Popescu and S. Zoia, *Next-to-next-to-leading order QCD corrections to $Wb\bar{b}$ production at the LHC*, *Phys. Rev. D* **106** (2022) 074016, [[2205.01687](#)].
- [4] S. Badger, H. B. Hartanto, J. Kryś and S. Zoia, *Two-loop leading-colour QCD helicity amplitudes for Higgs boson production in association with a bottom-quark pair at the LHC*, *JHEP* **11** (2021) 012, [[2107.14733](#)].
- [5] S. Badger, H. B. Hartanto, R. Poncelet, Z. Wu, Y. Zhang and S. Zoia, *Full-colour double-virtual amplitudes for associated production of a Higgs boson with a bottom-quark pair at the LHC*, [2412.06519](#).
- [6] F. Febres Cordero, G. Figueiredo, M. Kraus, B. Page and L. Reina, *Two-loop master integrals for leading-color $pp \rightarrow t\bar{t}H$ amplitudes with a light-quark loop*, *JHEP* **07** (2024) 084, [[2312.08131](#)].
- [7] B. Agarwal, G. Heinrich, S. P. Jones, M. Kerner, S. Y. Klein, J. Lang et al., *Two-loop amplitudes for $t\bar{t}H$ production: the quark-initiated N_f -part*, *JHEP* **05** (2024) 013, [[2402.03301](#)].
- [8] S. Devoto, M. Grazzini, S. Kallweit, J. Mazzitelli and C. Savoini, *Precise predictions for $t\bar{t}H$ production at the LHC: inclusive cross section and differential distributions*, [2411.15340](#).
- [9] S. Badger, H. B. Hartanto, J. Kryś and S. Zoia, *Two-loop leading colour helicity amplitudes for $W^\pm\gamma + j$ production at the LHC*, *JHEP* **05** (2022) 035, [[2201.04075](#)].
- [10] D. Kermanschah and M. Vicini, *N_f -contribution to the virtual correction for electroweak vector boson production at NNLO*, [2407.18051](#).
- [11] S. Badger, H. B. Hartanto, Z. Wu, Y. Zhang and S. Zoia, *Two-loop amplitudes for $\mathcal{O}(\alpha_s^2)$ corrections to $W\gamma\gamma$ production at the LHC*, [2409.08146](#).
- [12] D. Chicherin, V. Sotnikov and S. Zoia, *Pentagon functions for one-mass planar scattering amplitudes*, *JHEP* **01** (2022) 096, [[2110.10111](#)].

- [13] S. Abreu, D. Chicherin, H. Ita, B. Page, V. Sotnikov, W. Tschernow et al., *All Two-Loop Feynman Integrals for Five-Point One-Mass Scattering*, *Phys. Rev. Lett.* **132** (2024) 141601, [[2306.15431](#)].
- [14] S. Badger, M. Becchetti, E. Chaubey and R. Marzucca, *Two-loop master integrals for a planar topology contributing to $pp \rightarrow t\bar{t}j$* , *JHEP* **01** (2023) 156, [[2210.17477](#)].
- [15] S. Badger, M. Becchetti, N. Giraudo and S. Zoia, *Two-loop integrals for $t\bar{t}$ +jet production at hadron colliders in the leading colour approximation*, *JHEP* **07** (2024) 073, [[2404.12325](#)].
- [16] M. Hidding, *DiffExp, a Mathematica package for computing Feynman integrals in terms of one-dimensional series expansions*, *Comput. Phys. Commun.* **269** (2021) 108125, [[2006.05510](#)].
- [17] F. Moriello, *Generalised power series expansions for the elliptic planar families of Higgs + jet production at two loops*, *JHEP* **01** (2020) 150, [[1907.13234](#)].
- [18] A. V. Smirnov, *FIESTA4: Optimized Feynman integral calculations with GPU support*, *Comput. Phys. Commun.* **204** (2016) 189–199, [[1511.03614](#)].
- [19] S. Borowka, G. Heinrich, S. Jahn, S. P. Jones, M. Kerner, J. Schlenk et al., *pySecDec: a toolbox for the numerical evaluation of multi-scale integrals*, *Comput. Phys. Commun.* **222** (2018) 313–326, [[1703.09692](#)].
- [20] X. Liu and Y.-Q. Ma, *AMFlow: A Mathematica package for Feynman integrals computation via auxiliary mass flow*, *Comput. Phys. Commun.* **283** (2023) 108565, [[2201.11669](#)].
- [21] T. Armadillo, R. Bonciani, S. Devoto, N. Rana and A. Vicini, *Evaluation of Feynman integrals with arbitrary complex masses via series expansions*, *Comput. Phys. Commun.* **282** (2023) 108545, [[2205.03345](#)].
- [22] J. R. Ellis, M. K. Gaillard and D. V. Nanopoulos, *A Phenomenological Profile of the Higgs Boson*, *Nucl. Phys. B* **106** (1976) 292.
- [23] M. A. Shifman, A. I. Vainshtein, M. B. Voloshin and V. I. Zakharov, *Low-Energy Theorems for Higgs Boson Couplings to Photons*, *Sov. J. Nucl. Phys.* **30** (1979) 711–716.
- [24] B. A. Kniehl and M. Spira, *Low-energy theorems in Higgs physics*, *Z. Phys. C* **69** (1995) 77–88, [[hep-ph/9505225](#)].
- [25] C. Anastasiou, C. Duhr, F. Dulat, F. Herzog and B. Mistlberger, *Higgs Boson Gluon-Fusion Production in QCD at Three Loops*, *Phys. Rev. Lett.* **114** (2015) 212001, [[1503.06056](#)].

- [26] C. Anastasiou, C. Duhr, F. Dulat, E. Furlan, T. Gehrmann, F. Herzog et al., *High precision determination of the gluon fusion Higgs boson cross-section at the LHC*, *JHEP* **05** (2016) 058, [[1602.00695](#)].
- [27] L.-B. Chen, H. T. Li, H.-S. Shao and J. Wang, *Higgs boson pair production via gluon fusion at N^3LO in QCD*, *Phys. Lett. B* **803** (2020) 135292, [[1909.06808](#)].
- [28] L.-B. Chen, H. T. Li, H.-S. Shao and J. Wang, *The gluon-fusion production of Higgs boson pair: N^3LO QCD corrections and top-quark mass effects*, *JHEP* **03** (2020) 072, [[1912.13001](#)].
- [29] M. Grazzini, G. Heinrich, S. Jones, S. Kallweit, M. Kerner, J. M. Lindert et al., *Higgs boson pair production at NNLO with top quark mass effects*, *JHEP* **05** (2018) 059, [[1803.02463](#)].
- [30] H.-Y. Bi, L.-H. Huang, R.-J. Huang, Y.-Q. Ma and H.-M. Yu, *Electroweak Corrections to Double Higgs Production at the LHC*, *Phys. Rev. Lett.* **132** (2024) 231802, [[2311.16963](#)].
- [31] G. Heinrich, S. Jones, M. Kerner, T. Stone and A. Vestner, *Electroweak corrections to Higgs boson pair production: the top-Yukawa and self-coupling contributions*, *JHEP* **11** (2024) 040, [[2407.04653](#)].
- [32] H. Zhang, K. Schönwald, M. Steinhauser and J. Davies, *Electroweak corrections to $gg \rightarrow HH$: Factorizable contributions*, *PoS LL2024* (2024) 014, [[2407.05787](#)].
- [33] H. T. Li, Z.-G. Si, J. Wang, X. Zhang and D. Zhao, *Improved constraint on Higgs boson self-couplings with quartic and cubic power dependence in the cross section*, [[2407.14716](#)].
- [34] J. Davies, K. Schönwald, M. Steinhauser and H. Zhang, *Next-to-leading order electroweak corrections to $gg \rightarrow HH$ and $gg \rightarrow gH$ in the large- m_t limit*, *JHEP* **10** (2023) 033, [[2308.01355](#)].
- [35] J. Davies, G. Mishima, K. Schönwald, M. Steinhauser and H. Zhang, *Higgs boson contribution to the leading two-loop Yukawa corrections to $gg \rightarrow HH$* , *JHEP* **08** (2022) 259, [[2207.02587](#)].
- [36] E. W. N. Glover and J. J. van der Bij, *Higgs Boson Pair Production Via Gluon Fusion*, *Nucl. Phys. B* **309** (1988) 282–294.
- [37] S. Borowka, N. Greiner, G. Heinrich, S. P. Jones, M. Kerner, J. Schlenk et al., *Higgs Boson Pair Production in Gluon Fusion at Next-to-Leading Order with Full Top-Quark Mass Dependence*, *Phys. Rev. Lett.* **117** (2016) 012001, [[1604.06447](#)].
- [38] S. Borowka, N. Greiner, G. Heinrich, S. P. Jones, M. Kerner, J. Schlenk et al., *Full top quark mass dependence in Higgs boson pair production at NLO*, *JHEP* **10** (2016) 107, [[1608.04798](#)].

- [39] J. Baglio, F. Campanario, S. Glaus, M. Mühlleitner, M. Spira and J. Streicher, *Gluon fusion into Higgs pairs at NLO QCD and the top mass scheme*, *Eur. Phys. J. C* **79** (2019) 459, [[1811.05692](#)].
- [40] J. Baglio, F. Campanario, S. Glaus, M. Mühlleitner, J. Ronca, M. Spira et al., *Higgs-Pair Production via Gluon Fusion at Hadron Colliders: NLO QCD Corrections*, *JHEP* **04** (2020) 181, [[2003.03227](#)].
- [41] J. Baglio, F. Campanario, S. Glaus, M. Mühlleitner, J. Ronca and M. Spira, *$gg \rightarrow HH$: Combined uncertainties*, *Phys. Rev. D* **103** (2021) 056002, [[2008.11626](#)].
- [42] E. Bagnaschi, G. Degrossi and R. Gröber, *Higgs boson pair production at NLO in the POWHEG approach and the top quark mass uncertainties*, *Eur. Phys. J. C* **83** (2023) 1054, [[2309.10525](#)].
- [43] J. M. Campbell, G. De Laurentis and R. K. Ellis, *Analytic amplitudes for a pair of Higgs bosons in association with three partons*, *JHEP* **10** (2024) 230, [[2408.12686](#)].
- [44] J. Davies, K. Schönwald and M. Steinhauser, *Towards $gg \rightarrow HH$ at next-to-next-to-leading order: Light-fermionic three-loop corrections*, *Phys. Lett. B* **845** (2023) 138146, [[2307.04796](#)].
- [45] J. Davies, K. Schönwald, M. Steinhauser and M. Vitti, *Three-loop corrections to Higgs boson pair production: reducible contribution*, *JHEP* **08** (2024) 096, [[2405.20372](#)].
- [46] J. Mazzitelli, *NNLO study of top-quark mass renormalization scheme uncertainties in Higgs boson production*, *JHEP* **09** (2022) 065, [[2206.14667](#)].
- [47] S. Amoroso et al., *Les Houches 2019: Physics at TeV Colliders: Standard Model Working Group Report*, in *11th Les Houches Workshop on Physics at TeV Colliders: PhysTeV Les Houches*, 3, 2020, [[2003.01700](#)].
- [48] G. Wang, X. Xu, Y. Xu and L. L. Yang, *Next-to-leading order corrections for $gg \rightarrow ZH$ with top quark mass dependence*, *Phys. Lett. B* **829** (2022) 137087, [[2107.08206](#)].
- [49] L. Chen, J. Davies, G. Heinrich, S. P. Jones, M. Kerner, G. Mishima et al., *ZH production in gluon fusion at NLO in QCD*, *JHEP* **08** (2022) 056, [[2204.05225](#)].
- [50] J. Davies, G. Mishima, M. Steinhauser and D. Wellmann, *Double-Higgs boson production in the high-energy limit: planar master integrals*, *JHEP* **03** (2018) 048, [[1801.09696](#)].

- [51] J. Davies, G. Mishima, M. Steinhauser and D. Wellmann, *Double Higgs boson production at NLO in the high-energy limit: complete analytic results*, *JHEP* **01** (2019) 176, [[1811.05489](#)].
- [52] J. Davies, G. Heinrich, S. P. Jones, M. Kerner, G. Mishima, M. Steinhauser et al., *Double Higgs boson production at NLO: combining the exact numerical result and high-energy expansion*, *JHEP* **11** (2019) 024, [[1907.06408](#)].
- [53] J. Davies, G. Mishima, K. Schönwald and M. Steinhauser, *Analytic approximations of $2 \rightarrow 2$ processes with massive internal particles*, *JHEP* **06** (2023) 063, [[2302.01356](#)].
- [54] X. Xu and L. L. Yang, *Towards a new approximation for pair-production and associated-production of the Higgs boson*, *JHEP* **01** (2019) 211, [[1810.12002](#)].
- [55] G. Wang, Y. Wang, X. Xu, Y. Xu and L. L. Yang, *Efficient computation of two-loop amplitudes for Higgs boson pair production*, *Phys. Rev. D* **104** (2021) L051901, [[2010.15649](#)].
- [56] R. Bonciani, G. Degrossi, P. P. Giardino and R. Gröber, *Analytical Method for Next-to-Leading-Order QCD Corrections to Double-Higgs Production*, *Phys. Rev. Lett.* **121** (2018) 162003, [[1806.11564](#)].
- [57] R. Gröber, A. Maier and T. Rauh, *Reconstruction of top-quark mass effects in Higgs pair production and other gluon-fusion processes*, *JHEP* **03** (2018) 020, [[1709.07799](#)].
- [58] M. Beneke and V. A. Smirnov, *Asymptotic expansion of Feynman integrals near threshold*, *Nucl. Phys.* **B522** (1998) 321–344, [[hep-ph/9711391](#)].
- [59] V. A. Smirnov, *Asymptotic expansions in limits of large momenta and masses*, *Commun. Math. Phys.* **134** (1990) 109–137.
- [60] V. A. Smirnov, *Asymptotic expansions in momenta and masses and calculation of Feynman diagrams*, *Mod. Phys. Lett. A* **10** (1995) 1485–1500, [[hep-th/9412063](#)].
- [61] V. A. Smirnov, *Applied asymptotic expansions in momenta and masses*, *Springer Tracts Mod. Phys.* **177** (2002) 1–262.
- [62] C. W. Bauer, S. Fleming, D. Pirjol and I. W. Stewart, *An Effective field theory for collinear and soft gluons: Heavy to light decays*, *Phys. Rev. D* **63** (2001) 114020, [[hep-ph/0011336](#)].
- [63] C. W. Bauer, D. Pirjol and I. W. Stewart, *Soft collinear factorization in effective field theory*, *Phys. Rev. D* **65** (2002) 054022, [[hep-ph/0109045](#)].

- [64] C. W. Bauer, S. Fleming, D. Pirjol, I. Z. Rothstein and I. W. Stewart, *Hard scattering factorization from effective field theory*, *Phys. Rev. D* **66** (2002) 014017, [[hep-ph/0202088](#)].
- [65] M. Beneke, A. P. Chapovsky, M. Diehl and T. Feldmann, *Soft collinear effective theory and heavy to light currents beyond leading power*, *Nucl. Phys. B* **643** (2002) 431–476, [[hep-ph/0206152](#)].
- [66] M. Beneke and T. Feldmann, *Multipole expanded soft collinear effective theory with nonAbelian gauge symmetry*, *Phys. Lett. B* **553** (2003) 267–276, [[hep-ph/0211358](#)].
- [67] B. Jantzen, *Foundation and generalization of the expansion by regions*, *JHEP* **12** (2011) 076, [[1111.2589](#)].
- [68] T. Y. Semenova, A. V. Smirnov and V. A. Smirnov, *On the status of expansion by regions*, *Eur. Phys. J. C* **79** (2019) 136, [[1809.04325](#)].
- [69] V. A. Smirnov, *Simplifying the large-mass expansion of Feynman integrals*, *Theor. Math. Phys.* **219** (2024) 986–991, [[2307.00387](#)].
- [70] Y. Ma, *Identifying regions in wide-angle scattering via graph-theoretical approaches*, *JHEP* **09** (2024) 197, [[2312.14012](#)].
- [71] M. Borinsky, *Tropical Monte Carlo quadrature for Feynman integrals*, *Ann. Inst. H. Poincaré D Comb. Phys. Interact.* **10** (2023) 635–685, [[2008.12310](#)].
- [72] M. Borinsky, H. J. Munch and F. Tellander, *Tropical Feynman integration in the Minkowski regime*, *Comput. Phys. Commun.* **292** (2023) 108874, [[2302.08955](#)].
- [73] E. Gardi, F. Herzog, S. Jones, Y. Ma and J. Schlenk, *The on-shell expansion: from Landau equations to the Newton polytope*, *JHEP* **07** (2023) 197, [[2211.14845](#)].
- [74] E. Gardi, F. Herzog, S. Jones and Y. Ma, *Dissecting polytopes: Landau singularities and asymptotic expansions in $2 \rightarrow 2$ scattering*, *JHEP* **08** (2024) 127, [[2407.13738](#)].
- [75] A. A. Penin, *High-Energy Limit of Quantum Electrodynamics beyond Sudakov Approximation*, *Phys. Lett. B* **745** (2015) 69–72, [[1412.0671](#)].
- [76] T. Liu, A. A. Penin and N. Zerf, *Three-loop quark form factor at high energy: the leading mass corrections*, *Phys. Lett. B* **771** (2017) 492–496, [[1705.07910](#)].
- [77] T. Liu and A. A. Penin, *High-Energy Limit of QCD beyond the Sudakov Approximation*, *Phys. Rev. Lett.* **119** (2017) 262001, [[1709.01092](#)].

- [78] T. Liu and A. Penin, *High-Energy Limit of Mass-Suppressed Amplitudes in Gauge Theories*, *JHEP* **11** (2018) 158, [[1809.04950](#)].
- [79] A. A. Penin, *High energy limit of QCD beyond Sudakov approximation*, *PoS LL2018* (2018) 081.
- [80] J. Wang, *Resummation of double logarithms in loop-induced processes with effective field theory*, [1912.09920](#).
- [81] Z. L. Liu and M. Neubert, *Factorization at subleading power and endpoint-divergent convolutions in $h \rightarrow \gamma\gamma$ decay*, *JHEP* **04** (2020) 033, [[1912.08818](#)].
- [82] Z. L. Liu, B. Mecaj, M. Neubert, X. Wang and S. Fleming, *Renormalization and Scale Evolution of the Soft-Quark Soft Function*, *JHEP* **07** (2020) 104, [[2005.03013](#)].
- [83] Z. L. Liu, B. Mecaj, M. Neubert and X. Wang, *Factorization at subleading power and endpoint divergences in $h \rightarrow \gamma\gamma$ decay. Part II. Renormalization and scale evolution*, *JHEP* **01** (2021) 077, [[2009.06779](#)].
- [84] C. Anastasiou and A. Penin, *Light Quark Mediated Higgs Boson Threshold Production in the Next-to-Leading Logarithmic Approximation*, *JHEP* **07** (2020) 195, [[2004.03602](#)].
- [85] T. Liu, S. Modi and A. A. Penin, *Higgs boson production and quark scattering amplitudes at high energy through the next-to-next-to-leading power in quark mass*, *JHEP* **02** (2022) 170, [[2111.01820](#)].
- [86] Z. L. Liu, M. Neubert, M. Schnubel and X. Wang, *Factorization at next-to-leading power and endpoint divergences in $gg \rightarrow h$ production*, *JHEP* **06** (2023) 183, [[2212.10447](#)].
- [87] Z. L. Liu, B. Mecaj, M. Neubert and X. Wang, *Factorization at subleading power, Sudakov resummation, and endpoint divergences in soft-collinear effective theory*, *Phys. Rev. D* **104** (2021) 014004, [[2009.04456](#)].
- [88] T. Liu, A. A. Penin and A. Rehman, *Light quark mediated Higgs boson production in association with a jet at the next-to-next-to-leading order and beyond*, *JHEP* **04** (2024) 031, [[2402.18625](#)].
- [89] M. Beneke, C. Bobeth and R. Szafron, *Enhanced electromagnetic correction to the rare $B_{s,d}$ meson decay $B_{s,d} \rightarrow \mu^+\mu^-$* , *Phys. Rev. Lett.* **120** (2018) 011801, [[1708.09152](#)].
- [90] M. Beneke, C. Bobeth and R. Szafron, *Power-enhanced leading-logarithmic QED corrections to $B_q \rightarrow \mu^+\mu^-$* , *JHEP* **10** (2019) 232, [[1908.07011](#)].

- [91] M. Schnubel, *Two applications of effective field theory: factorisation of $gg \rightarrow h$ in SCET & flavour physics of ALPs*, Ph.D. thesis, Mainz U., 9, 2023.
10.25358/openscience-9558.
- [92] G. Mishima, *High-Energy Expansion of Two-Loop Massive Four-Point Diagrams*, *JHEP* **02** (2019) 080, [[1812.04373](#)].
- [93] R. N. Lee and A. A. Pomeransky, *Critical points and number of master integrals*, *JHEP* **11** (2013) 165, [[1308.6676](#)].
- [94] B. Jantzen, A. V. Smirnov and V. A. Smirnov, *Expansion by regions: revealing potential and Glauber regions automatically*, *Eur. Phys. J. C* **72** (2012) 2139, [[1206.0546](#)].
- [95] G. Heinrich, S. Jahn, S. P. Jones, M. Kerner, F. Langer, V. Magerya et al., *Expansion by regions with pySecDec*, *Comput. Phys. Commun.* **273** (2022) 108267, [[2108.10807](#)].
- [96] T. Becher, P. Hager, S. Jaskiewicz, M. Neubert and D. Schwienbacher, *Factorization restoration through Glauber gluons*, [2408.10308](#).
- [97] T. Engel, *Muon-Electron Scattering at NNLO*, Ph.D. thesis, Zurich U., 2022.
[2209.11110](#).
- [98] M. Beneke, *Helmholtz International Summer School on Heavy Quark Physics, Dubna*, 2005.
- [99] T. Becher and M. Neubert, *Drell-Yan Production at Small q_T , Transverse Parton Distributions and the Collinear Anomaly*, *Eur. Phys. J. C* **71** (2011) 1665, [[1007.4005](#)].
- [100] S. Jones and Y. Ulrich, in preparation.
- [101] J. Klappert, F. Lange, P. Maierhöfer and J. Usovitsch, *Integral reduction with Kira 2.0 and finite field methods*, *Comput. Phys. Commun.* **266** (2021) 108024, [[2008.06494](#)].
- [102] M. Beneke, M. Garny, R. Szafron and J. Wang, *Anomalous dimension of subleading-power N -jet operators*, *JHEP* **03** (2018) 001, [[1712.04416](#)].
- [103] M. Beneke, M. Garny, R. Szafron and J. Wang, *Anomalous dimension of subleading-power N -jet operators. Part II*, *JHEP* **11** (2018) 112, [[1808.04742](#)].
- [104] M. Beneke, M. Garny, R. Szafron and J. Wang, *Violation of the Kluberg-Stern-Zuber theorem in SCET*, *JHEP* **09** (2019) 101, [[1907.05463](#)].

- [105] I. Feige, D. W. Kolodrubetz, I. Moulton and I. W. Stewart, *A Complete Basis of Helicity Operators for Subleading Factorization*, *JHEP* **11** (2017) 142, [[1703.03411](#)].
- [106] I. Moulton, I. W. Stewart and G. Vita, *A subleading operator basis and matching for $gg \rightarrow H$* , *JHEP* **07** (2017) 067, [[1703.03408](#)].
- [107] R. J. Hill and M. Neubert, *Spectator interactions in soft collinear effective theory*, *Nucl. Phys. B* **657** (2003) 229–256, [[hep-ph/0211018](#)].
- [108] M. Beneke, M. Garry, S. Jaskiewicz, R. Szafron, L. Vernazza and J. Wang, *Large- x resummation of off-diagonal deep-inelastic parton scattering from d -dimensional refactorization*, *JHEP* **10** (2020) 196, [[2008.04943](#)].
- [109] M. Beneke, M. Garry, S. Jaskiewicz, J. Strohm, R. Szafron, L. Vernazza et al., *Next-to-leading power endpoint factorization and resummation for off-diagonal “gluon” thrust*, *JHEP* **07** (2022) 144, [[2205.04479](#)].
- [110] G. Bell, P. B er and T. Feldmann, *Muon-electron backward scattering: a prime example for endpoint singularities in SCET*, *JHEP* **09** (2022) 183, [[2205.06021](#)].
- [111] A. K. Leibovich, Z. Ligeti and M. B. Wise, *Comment on quark masses in SCET*, *Phys. Lett. B* **564** (2003) 231–234, [[hep-ph/0303099](#)].
- [112] M. Beneke, A. Broggio, M. Garry, S. Jaskiewicz, R. Szafron, L. Vernazza et al., *Leading-logarithmic threshold resummation of the Drell-Yan process at next-to-leading power*, *JHEP* **03** (2019) 043, [[1809.10631](#)].
- [113] M. Beneke, A. Broggio, S. Jaskiewicz and L. Vernazza, *Threshold factorization of the Drell-Yan process at next-to-leading power*, *JHEP* **07** (2020) 078, [[1912.01585](#)].
- [114] M. Beneke, M. Garry, S. Jaskiewicz, R. Szafron, L. Vernazza and J. Wang, *Leading-logarithmic threshold resummation of Higgs production in gluon fusion at next-to-leading power*, *JHEP* **01** (2020) 094, [[1910.12685](#)].
- [115] A. Broggio, S. Jaskiewicz and L. Vernazza, *Threshold factorization of the Drell-Yan quark-gluon channel and two-loop soft function at next-to-leading power*, *JHEP* **12** (2023) 028, [[2306.06037](#)].
- [116] A. A. Penin, *Two-loop photonic corrections to massive Bhabha scattering*, *Nucl. Phys. B* **734** (2006) 185–202, [[hep-ph/0508127](#)].
- [117] A. Mitov and S. Moch, *The Singular behavior of massive QCD amplitudes*, *JHEP* **05** (2007) 001, [[hep-ph/0612149](#)].
- [118] T. Becher and K. Melnikov, *Two-loop QED corrections to Bhabha scattering*, *JHEP* **06** (2007) 084, [[0704.3582](#)].

- [119] T. Engel, C. Gnendiger, A. Signer and Y. Ulrich, *Small-mass effects in heavy-to-light form factors*, *JHEP* **02** (2019) 118, [[1811.06461](#)].
- [120] G. Wang, T. Xia, L. L. Yang and X. Ye, *On the high-energy behavior of massive QCD amplitudes*, *JHEP* **05** (2024) 082, [[2312.12242](#)].
- [121] G. Wang, T. Xia, L. L. Yang and X. Ye, *Two-loop QCD amplitudes for $t\bar{t}H$ production from boosted limit*, *JHEP* **07** (2024) 121, [[2402.00431](#)].
- [122] T. Becher and M. Neubert, *On the Structure of Infrared Singularities of Gauge-Theory Amplitudes*, *JHEP* **06** (2009) 081, [[0903.1126](#)].
- [123] J. M. Henn, G. P. Korchemsky and B. Mistlberger, *The full four-loop cusp anomalous dimension in $\mathcal{N} = 4$ super Yang-Mills and QCD*, *JHEP* **04** (2020) 018, [[1911.10174](#)].
- [124] J.-Y. Chiu, A. Jain, D. Neill and I. Z. Rothstein, *A Formalism for the Systematic Treatment of Rapidity Logarithms in Quantum Field Theory*, *JHEP* **05** (2012) 084, [[1202.0814](#)].
- [125] J. A. M. Vermaseren, S. A. Larin and T. van Ritbergen, *The four loop quark mass anomalous dimension and the invariant quark mass*, *Phys. Lett. B* **405** (1997) 327–333, [[hep-ph/9703284](#)].
- [126] M. Neubert, *Renormalization-group improved calculation of the $B \rightarrow X_s \gamma$ branching ratio*, *Eur. Phys. J. C* **40** (2005) 165–186, [[hep-ph/0408179](#)].
- [127] S. Catani, *The Singular behavior of QCD amplitudes at two loop order*, *Phys. Lett. B* **427** (1998) 161–171, [[hep-ph/9802439](#)].
- [128] D. J. Broadhurst, N. Gray and K. Schilcher, *Gauge invariant on-shell $Z(2)$ in QED, QCD and the effective field theory of a static quark*, *Z. Phys. C* **52** (1991) 111–122.
- [129] R. Tarrach, *The Pole Mass in Perturbative QCD*, *Nucl. Phys. B* **183** (1981) 384–396.
- [130] F. Caola, A. Von Manteuffel and L. Tancredi, *Diphoton Amplitudes in Three-Loop Quantum Chromodynamics*, *Phys. Rev. Lett.* **126** (2021) 112004, [[2011.13946](#)].
- [131] P. Bargiela, F. Caola, A. von Manteuffel and L. Tancredi, *Three-loop helicity amplitudes for diphoton production in gluon fusion*, *JHEP* **02** (2022) 153, [[2111.13595](#)].
- [132] K. G. Chetyrkin, J. H. Kuhn and M. Steinhauser, *RunDec: A Mathematica package for running and decoupling of the strong coupling and quark masses*, *Comput. Phys. Commun.* **133** (2000) 43–65, [[hep-ph/0004189](#)].

- [133] F. Herren and M. Steinhauser, *Version 3 of RunDec and CRunDec*, *Comput. Phys. Commun.* **224** (2018) 333–345, [[1703.03751](#)].
- [134] P. Marquard, A. V. Smirnov, V. A. Smirnov, M. Steinhauser and D. Wellmann, *$\overline{\text{MS}}$ -on-shell quark mass relation up to four loops in QCD and a general $SU(N)$ gauge group*, *Phys. Rev. D* **94** (2016) 074025, [[1606.06754](#)].
- [135] M. Cepeda et al., *Report from Working Group 2: Higgs Physics at the HL-LHC and HE-LHC*, *CERN Yellow Rep. Monogr.* **7** (2019) 221–584, [[1902.00134](#)].
- [136] D. Binosi, J. Collins, C. Kaufhold and L. Theussl, *JaxoDraw: A Graphical user interface for drawing Feynman diagrams. Version 2.0 release notes*, *Comput. Phys. Commun.* **180** (2009) 1709–1715, [[0811.4113](#)].
- [137] W. Bernreuther and W. Wetzel, *Decoupling of Heavy Quarks in the Minimal Subtraction Scheme*, *Nucl. Phys. B* **197** (1982) 228–236.
- [138] P. Bärnreuther, M. Czakon and P. Fiedler, *Virtual amplitudes and threshold behaviour of hadronic top-quark pair-production cross sections*, *JHEP* **02** (2014) 078, [[1312.6279](#)].